

1
2
3
4
5
6
7
8
9
10
11
12
13**HAI –****A new, airborne, absolute, twin dual-channel, multi-phase TDLAS-hygrometer****Bernhard Buchholz^{1,2,5}, Armin Afchine⁴, Alexander Klein¹,
Cornelius Schiller⁴, Martina Krämer⁴, Volker Ebert^{1,2,3}**¹ Physikalisch-Technische Bundesanstalt Braunschweig, Germany² Physikalisch Chemisches Institut, Universität Heidelberg, Germany³ Center of Smart Interfaces, Technische Universität Darmstadt, Germany⁴ Forschungszentrum Jülich, IEK-7, Germany⁵currently at Department of Civil and Environmental Engineering, Princeton University, USA.

†deceased

Corresponding author: volker.ebert@ptb.de

14

Abstract15
16
17
18
19
20
21
22
23
24
25
26
27
28
29
30
31
32
33

The novel Hygrometer for Atmospheric Investigations (HAI) realizes a unique concept for simultaneous gas-phase and total (gas-phase + evaporated cloud particles) water measurement. It has been developed and successfully employed for the first time on the German HALO research aircraft. This new instrument combines direct Tunable Diode Laser Absorption Spectroscopy (dTDLAS) with a first-principle evaluation method to allow absolute water vapor measurements without any initial or repetitive sensor calibration using a reference gas or a reference humidity generator. HAI contains two completely independent dual-channel (closed-path, open-path) spectrometers, one at 1.4 μm and one at 2.6 μm , which allow together to cover the entire atmospheric H_2O range from 1 to 40 000 ppmv with a single instrument. Both spectrometers comprise each a separate, wavelength-individual extractive, closed-path cell for total water (ice and gas-phase) measurements. Additionally, both spectrometers couple light into a common, open-path-cell outside of the aircraft fuselage for a direct, sampling-free and contactless determination of the gas-phase water content. This novel twin dual-channel setup allows for the first time multiple self-validation functions i.e. in particular a reliable, direct, in-flight validation of the open-path channels. During the first field campaigns, the in-flight deviations between the independent and calibration-free channels (i.e. closed-path to closed-path and open-path to closed-path) were on average in the 2% range. Further, the fully autonomous HAI hygrometer allows measurements up to 240 Hz with a minimal integration time of 1.4 ms. The best precision is achieved by the 1.4 μm closed-path cell at 3.8 Hz (0.18 ppmv) and by the 2.6 μm closed-path cell at 13 Hz (0.055 ppmv). The requirements, design, operation principle and in-flight performance of the hygrometer are described in this work.

34

1. Introduction35
36
37
38
39
40
41

Water vapor is in many ways one of the most important measurand for atmospheric investigations (Ludlam, 1980; Möller et al., 2011; Ravishankara, 2012). Water is the most important greenhouse gas (Kiehl and Trenberth, 1997), and known as a key atmospheric coupling element of almost all microscopic (e.g. droplets/ice crystals formation), macroscopic (e.g. clouds/precipitation) and global processes (e.g. hydrological cycle). Therefore, it is strongly related to the numerous highly relevant topics of atmospheric science and closely related to “climate change” (Held and Soden, 2000; Houghton, 2009; Kiehl and Trenberth, 1997; Maycock et al., 2011). Unsurprisingly, numerous water vapor studies have been carried out targeting its



42 atmospheric trends and variability (Lu and Takle, 2010; McCarthy et al., 2009; Ross and Elliott, 1996; Scherer
43 et al., 2008; Trenberth et al., 2005; Xie et al., 2011), its influence on transport models (Kiemle et al., 2012;
44 Schäfler et al., 2010), or its impact on radiation balance models (Lockwood, 1990; Ramanathan et al., 1989;
45 Schneider, 1972). One reason for the high complexity of atmospheric water vapor is that it is one of the few
46 atmospheric molecules that appears in all three phases. Water in the gas-phase is a very strong infrared
47 absorber and significantly impacts atmospheric energy fluxes through latent heat transfers by the different
48 phase transitions. Condensation to the liquid phase or freezing to solid particles leads to effective scattering
49 of solar radiation, which directly raises links to the formation process of cirrus clouds (Krämer et al., 2009;
50 Spichtinger et al., 2004). These relationships show the complexity from a theoretical as well as a modeling
51 point of view. Today, however, the quality e.g. particularly accuracy and comparability of atmospheric
52 water measurements frequently limit a better understanding of key atmospheric processes (Krämer et al.,
53 2009; Peter et al., 2006; Scherer et al., 2008; Sherwood et al., 2014). Despite the outlined importance and the
54 large effort invested in the developments of hygrometers in recent years, water vapor remains a target mol-
55 ecule that is very difficult to measure accurately.

56 Several major issues exacerbate water vapor measurements. Atmospheric water vapor encompasses a very
57 large concentration range: 3 – 40 000 ppmv from troposphere up to the lower stratosphere. The spatial fluc-
58 tuations of H₂O in the atmosphere are high, which leads on fast aircraft (approx. 800 km/s cruising speed) to
59 highly dynamic H₂O variations of up to several 1000 ppmv/s in the gas-phase and up to several
60 10 000 ppmv/s for total water measurements. These issues require, especially for aircraft based hygrome-
61 ters, very high time resolution in combination with very high precision and accuracy. Additionally, since
62 water vapor readily changes from one phase to the other, it would be extremely helpful if hygrometer were
63 able to differentiate between the phases or could differentiate at least between water vapor and total water
64 in order to minimize systematic uncertainties caused by the sampling process. Last but not least, water va-
65 por is very effectively absorbed from nearly any surface. This challenges in a highly complex manner not
66 only the entire gas sampling system but also the calibration infrastructure which is typically required for
67 most hygrometers. By waiving the entire calibration process, special hygrometers (Wolfrum et al., 2011)
68 circumvent all calibration related issues efficiently which will explained in chapter 3.2.

69 This brief compilation illustrates the complex challenges associated with developing a water vapor instru-
70 ment, especially if it should be able to measure in tropospheric and stratospheric atmospheric conditions.
71 Numerous (mostly single-channel) hygrometers have been developed in the last decades with various ad-
72 vantages and drawbacks (see (Wiederhold, 1997) and e.g. (Buck, 1985; Busen and Buck, 1995; Cerni, 1994;
73 Desjardins et al., 1989; Diskin et al., 2002; Durrý et al., 2008; Ebert et al., 2000b; Gurlit et al., 2005; Hansford
74 et al., 2006; Helten et al., 1998; Hunsmann et al., 2008; Karpechko et al., 2014; Kley and Stone, 1978; May,
75 1998; Meyer et al., 2015; Ohtaki and Matsui, 1982; Roths and Busen, 1996; Salasmaa and Kostamo, 1986;
76 Schiff et al., 1994; Silver and Hovde, 1994b, 1994a; Thornberry et al., 2014; Webster et al., 2004; Zöger et al.,
77 1999a, 1999b)). Consequently, the question should be raised from the opposite point of view: What are the
78 important and required properties to be covered and combined for a near-universal “Hygrometer for At-
79 mospheric Investigation” to serve as an innovative and cutting-edge tool to explore open and new scientific
80 questions related to atmospheric water vapor?



81

82 **2. Requirements for HAI, a “Hygrometer for Atmospheric Investigation”**83 **2.1. Specific instrumental boundary conditions defined by the atmosphere**

84 Currently, atmospheric water vapor data are generated from two instrument types: Remote sensing ap-
85 proaches (like satellites (Oelhaf et al., 2004) or ground-based – often FTIR based - monitoring stations
86 (Zachariassen et al., 2003)) or in-situ hygrometers deployed directly inside of the environment to be meas-
87 ured. The latter are roughly separated in ground-base “weather stations”, balloon-borne radiosondes
88 (Miloshevich et al., 2006) and hygrometers on airborne carriers like aircraft (Marenco et al., 1998). While
89 ground-based stations permanently provide local information, radiosondes deliver “only” one point like
90 vertical profile per ascend/ descend but for heights up to 50 km above ground. Airborne vehicles like air-
91 craft and helicopters, however, combine the possibility for arbitrary flight paths and localized measure-
92 ments, e.g. for cloud investigations, with a beneficial long operation range. In particular the most modern
93 research aircrafts such as the German HALO aircraft (Anon, 2014; Krautstrunk and Giez, 2012) or the US
94 American HIAPER (Anon, n.d.) bridge the gap and combine broad spatial coverage (> 10 000 km), high
95 altitudes (up to 15 km), and large payloads of up to 3000 kg payload, in a favorable pressurized, and air-
96 conditioned cabin. The relatively high traveling speed of these aircraft (of up to 230 m/sec), however, also
97 causes disadvantageous influences on the measurements themselves, which are difficult to take care of
98 compared to the very slowly moving (low m/sec range), quasi-static balloon-borne radiosondes. Even rela-
99 tively simple meteorological variables such as air temperature and pressure need complex retrieval algo-
100 rithms (Giez, 2012) if measured on a high speed aircraft. In short, aircraft in the contemporary working
101 equipment are indispensable for both the investigation of spatially confined effects too small to retrieve
102 from remote sensing data and the validation of the remote sensing instruments (Oelhaf et al., 2004). It is
103 highly desirable for an airborne system to be constructed in a way that it operates on the ground in the
104 same manner as in flight and that every change of environment and “boundary conditions” of the instru-
105 ment is logged. This allows, besides multipliable deployments e.g. in ground based stations, extensive vali-
106 dation as well as laboratory comparisons with other instruments and avoids systematic, barely detectable
107 deviations only occurring in flight. This notion related to water vapor leads directly into the everlasting
108 discussion about sampling via open-path systems operation in the free flow versus closed-path systems
109 extracting the air to be analyzed into the instrument. Open-path hygrometers offer numerous great benefits
110 such as: the prevention of any sampling errors or uncertainties (caused by surface absorbing effects) as well
111 as the high response time that is limited only by the transfer functions of optical or electrical components
112 but not by the gas exchange rate. The latter circumvents the complicated and adulterant deconvolution of
113 smoothing effects with time-response functions caused by a sampling system. On the other hand, the
114 boundary conditions such as gas pressure and gas temperature as well as possible spatial inhomogeneities
115 of both parameters are difficult to accurately take into account for an open-path system. Additionally, an
116 airborne open-path sensor has to operate in harsh boundary conditions, i.e. over a large range of tempera-



117 tures (-80 to 50 °C), pressures (70 to 1000 hPa), for large ram pressures (900 km/h gas velocity) and mechan-
118 ical stress through accretion of ice or liquid water.

119 The major problem of all present open-path systems is their highly complex calibration, or even just valida-
120 tion, since realistic flight conditions, in particular the dynamics, are extremely difficult to realize in the lab
121 with sufficient accuracy. A direct metrological link to test the inflight performance, e.g. a dynamic calibra-
122 tion facility for open-path hygrometers, is therefore missing.

123 Closed-path systems, on the other side, are simply installed inside an air-conditioned cabin, in a much more
124 protected environment. Gas is sampled with a suitable inlet and led via a tubing system to an “internal”
125 measurement chamber, such as an optical absorption cell or a suitable “cavity”, e.g. for a dew point mirror
126 hygrometer. On one hand, it is much easier to accurately control and maintain the physical boundary con-
127 ditions of the sample gas, e.g. temperature, pressure, flow, etc. in the measurement volume. On the other
128 hand, it is difficult to ensure and maintain a representative sampling process and to quantify and correct
129 sampling related deviations. These maybe caused by adsorption and desorption effects, which occur on all
130 surfaces of the sampling system, and have to be carefully minimized by heated (HAI ≈80 °C) stainless steel
131 sampling pipes, along with an instrument design ensuring high gas flows (HAI ≈100 liter/min) under all
132 flight conditions.

133 Gas-phase H₂O measurements in clouds are often carried out via backward facing sampling inlets. But such
134 inlets are readily sampling small liquid or solid water particles possibly causing systematically positive
135 offsets. For every H₂O measurement using airborne extractive (=closed-path) instruments on aircrafts, it
136 needs to be taken into account that the instruments response reflects contributions from the sensor element
137 itself as well as the sampling/tubing system and their dynamic properties. One indisputable, major ad-
138 vantage of typical extractive instruments is the possibility for careful tests outside of the aircraft, i.e. in a
139 hangar or laboratory. But, to take full advantage of this, it is desirable for a sophisticated instrument to in-
140 tegrate supervising and monitoring functions in a way that a performance comparable to the laboratory can
141 be ensured during any inflight situation. This generates the great benefit of transferring the performance
142 from the laboratory to the field situation, quite similar how a metrological transfer standard is typically
143 used. This directly reinforces the question, how to assess the accuracy of airborne hygrometers.

144 2.2. Accuracy and state of the art instrumentation

145 In general, the highest measurement and preparation accuracy is realized by the validated primary stand-
146 ards of national metrology institutes such as PTB (Germany) or NIST (USA). The international, metrological
147 water vapor scale is defined by traceable primary water vapor generators (Brewer et al., 2011). The mixing
148 ratio range, required to cover the entire tropospheric and stratospheric coverage of about 3 - 40000 ppmv, is
149 realized by a combination of generators based on different physical principles. Their typical uncertainty is
150 in the order of 0.5% relative, but varies with the physical principle used and their realization (Brewer et al.,
151 2011; Buchholz et al., 2014a; Mackrodt, 2012). In other words, it is not possible to validate any hygrometer
152 with better accuracy due to the lack of a suitable accurate reference.



153 Comparing the available metrological accuracy to some results from field comparisons of airborne hygrom-
154 eters demonstrates the large potential for improvement. For example, long-term (> 10 years) change studies
155 of stratospheric H₂O (Oltmans and Hofmann, 1995; Rosenlof et al., 2001; Solomon et al., 2010) suffer from
156 significant, difficult to quantify relative deviations between different instruments in the range of 50–100%
157 (Fahey et al., 2014; Peter et al., 2006; Vömel et al., 2007) which recent studies such as (Rollins et al., 2014)
158 confirm (± 40 –50% for < 3 ppmv and ± 20 % for > 3 ppmv). Radiosonde comparisons with polymer sensors and
159 chilled dew point mirror hygrometer, covering the entire troposphere and lower stratosphere region such
160 as (Miloshevich et al., 2006), show averaged overall agreement in the 10% range (but also, local deviations
161 in the 30% range). These deviations are quite common for many airborne campaign results e.g. (Smit et al.,
162 2014) and become even worse when focusing on the relative deviations in regions containing highly varia-
163 ble H₂O structures. Hence in 2007, an international comparison exercise, “AquaVIT” (Fahey and Gao, 2009),
164 was organized to compare the world’s best airborne hygrometers under well-controlled, quasi-static,
165 equivalent conditions to evaluate the accuracy under well controlled laboratory conditions, without the
166 influence of any typical airborne sampling and dynamic effects. AquaVIT comprised 22 hygrometers (tuna-
167 ble diode laser spectrometers, TDL, dew or frost point mirror hygrometers, D/FPH, Lyman alpha fluores-
168 cence and absorption hygrometers, LAFH and other principles) from 17 international research groups. The
169 instruments were categorized in well validated “core” instruments (APicT, FISH, FLASH, HWV, JLH, CFH,
170 see (Fahey and Gao, 2009) for details) and “younger, less mature” non-core instruments. Even the core-
171 hygrometers deviated in the important 1 to 150 ppmv WVMR range by up to ± 10 % from the mean. In oth-
172 er words, core instruments differed by up to 20% from each other, even under quasi-static conditions. Oth-
173 er, less representative and extensive comparisons such as (Hoff, 2009; Mangold and Wodca Team, 2003)
174 yielded similar results.

175 Of course, the assessment of the required accuracy depends strongly on the purpose of the data. In terms of
176 climatologies and strongly averaged or coarse validation studies such deviations can be acceptable, but as
177 far as e.g. retrieval models for satellite data improve, such uncertainties and deviations can become critical.
178 In many other cases such as the currently often discussed atmospheric super saturations (Peter et al., 2006),
179 the instrument uncertainties prevent deeper investigations and therefore a better understanding. Reconsid-
180 ering the entire situation and perceiving that after so much development effort over the past decades these
181 deviations remain quite high, leads to the inevitable question of the concealed, common impact factors.
182 Contemplating the typical metrological efforts needed at national metrology institutes (NMI) to generate an
183 accurately humidified gas stream (with a sub-percent uncertainty) suggests that the uncertainties generated
184 by typical calibration processes under field conditions could be a major contribution to these hygrometers
185 deviations found in AquaVIT and other studies. In particular, comparing the performance and strategies of
186 lab-based, metrological and portable field calibration facilities (Friehe et al., 1986; Helten et al., 1998;
187 Podolske et al., 2003; Smit et al., 2000; Smorgon et al., 2014; Zöger et al., 1999b) show three significant dis-
188 crepancies: required time for calibration, frequency of calibration, and traceability of the humidity reference
189 itself. Calibrations in the low concentration ranges at NMIs take several hours up to days per individual
190 humidity value. During airborne campaigns, however, calibrations often *have* to be realized (for practical
191 reasons) in a short time, certainly less than a few hours (max) for a large number of concentration steps



192 often including several pressure levels, thereby taking the obvious risk that the instrument/reference is not
193 fully stabilized or equilibrated. Ideally, the time between two calibrations should be shorter than the ex-
194 pected time required for a drift/change exceeding the boundaries of the instrument uncertainties. Some
195 airborne instruments require for the same reason calibrations before and after each flight in order to inter-
196 polate between both calibrations (Zöger et al., 1999b). Some even work with in-flight calibrations
197 (Kaufmann et al., 2016) sacrificing measurement time and shifting the accuracy issue to the necessary air-
198 borne H₂O-source. Undoubtedly, many of these instruments have benefits e.g. in terms of precision, space,
199 weight, prime cost etc., which justifies the calibration effort. However, vice versa, it is condoned that the
200 calibration process is hampered and turns out to be the major influence on the accuracy of such a sensor.
201 Lastly, it seems necessary to implement a traceable link to the metrological humidity scales to improve the
202 overall accuracy of airborne hygrometry (Joint Committee for Guides in Metrology (JCGM), 2009). By real-
203 izing an unbroken chain of calibrations, it is possible to link the instrument performance and the metrologi-
204 cal water scale respectively the SI system of units. This also guarantees an accurate measure-
205 ment/generation value with defined uncertainties.

206 To summarize: Fulfilling all these demands in the field similar like in a NMI laboratory is a tough task.
207 However, as discussed later, many of the covered issues can be circumvented using first principle tech-
208 niques like dTDLAS (Ebert and Wolfrum, 1994; Schulz et al., 2007) to realize optical, absolute hygrometers
209 which avoid over certain defined operating ranges any water vapor sensor calibration.

210 From a user's point of view, precision and response time of an airborne hygrometer appears equivalent to
211 accuracy if he is interested in fine structure resolving data. Precision and response time are under certain
212 circumstances reciprocally correlated to each other (Allan, 1966). Typical figures for response time of air-
213 borne hygrometer in the literature are 0.5 – 1 Hz (Petersen et al., 2010; Szakáll et al., 2004; Zöger et al.,
214 1999b); some instruments deliver faster data 4 Hz (Weinstock et al., 1994) or special instruments up to 25 Hz
215 (Zondlo et al., 2010). Typical precisions at 1 Hz are in 0.1-0.2 ppmv range (Sargent et al., 2013; Zöger et al.,
216 1999b; Zondlo et al., 2010). While in the stratosphere (<10 ppm), the precision certainly can become a limit-
217 ing factor. This is much less the case inside clouds or within the troposphere, where frequent, very strong
218 spatial variations (up to 1000 ppmv per 100 m flightpath in the gas-phase, or up to 20000 ppmv per 100 m
219 during total H₂O phase) pose a larger problem. An instrument with a time response of just a few Hz causes
220 significant under-sampling which can lead to strong aliasing effects at the high velocities (approx. 700-
221 900 km/h) of many research aircrafts. Important under such conditions is the instrument's linearity to accu-
222 rately cover the entire H₂O concentration range up to five magnitudes for total water vapor measurements.

223 Numerous additional requirements have to be fulfilled by an airborne instrument to ensure a successful
224 operation. Due to the high operation costs for aircrafts and the high scientific demand, H₂O data have to be
225 measured continuously without any interruptions. The instrument thus has to be highly reliable, robust,
226 and require low maintenance. The restrictions in weight and space as associated with operation on an air-
227 craft result in the necessity for the device to be of a compact and lightweight construction. The utterly com-
228 plex and mandatory certification process (at least in Germany) quickly enforces an instrument design freeze
229 before a campaign; this results in very stiff constraints for improvements/repairs during a campaign.

230



231 **3. Design decisions and approach**

232 HAI reflects on these by providing four independent but coupled spectrometers in one single housing and
233 by simultaneously combining open- with closed-path measurements in one single instrument. For all
234 channels the evaluation is done with one common spectroscopic method: calibration-free direct Tunable
235 Diode Laser Absorption Spectroscopy (cal-free dTDLAS).
236

237 **3.1. Direct Tunable diode laser absorption spectroscopy (dTDLAS)**

238 The requirements for fast measurements and high chemical selectivity in combination with a robust and
239 small system calls to choose a contact-less, spectroscopic (hence optical) measurement technique rather than
240 contact-mediated sensing methods such as dew point mirror hygrometer (DPH) or capacitive polymer
241 sensors e.g. “Humicap” (Salasmaa and Kostamo, 1986; Smit et al., 2000). These are quite often used in air-
242 borne hygrometry and especially in meteorological environments (Anon, 2010; Busen and Buck, 1995;
243 Hansford et al., 2006; Wiederhold, 1997). Optical hygrometers can be set up to become quite immune to
244 hydrophilic/hydrophobic substances (unavoidable in the vicinity of aircraft) as well as particles (dust, soot,
245 ice, etc.) contained by the gas to be analyzed. These capabilities were e.g. extensively demonstrated via
246 measurements inside of combustion processes in industrial power plants (Ebert et al., 2000a; Schlosser et al.,
247 2002; Sun et al., 2013; Teichert et al., 2003). Even response times in the several 10 kHz range could be
248 demonstrated recently by (Witzel et al., 2013) for measurements in combustion engines.

249 Tunable diode laser absorption spectroscopy (TDLAS) is a powerful as well as versatile diagnostic tech-
250 nique which is frequently employed in the near infrared spectral range and led to numerous applications in
251 atmospheric hygrometry (Diskin et al., 2002; Fahey and Gao, 2009; Gurlit et al., 2005; May, 1998; Schiff et al.,
252 1994; Thornberry et al., 2014). Advantageous diode lasers properties are the very high spectral resolution
253 and power density, the continuous tuneability in combination with interesting technical features such as
254 low cost, very low size/weight/power consumption, long life time, excellent beam quality, and optical fiber
255 coupling to name just a few.

256 The typical setup and working principle of a TDLAS instrument has been frequently described in detail
257 (Lackner, 2011; Schiff et al., 1994; Schulz et al., 2007; Werle, 1998). Therefore, only the HAI design relevant
258 topics are discussed here. Important for an understanding of the novel HAI instrument is the classification
259 of TDLAS instruments by their optical detection schemes in classical single- (Ebert et al., 2000b) or multi-
260 path (Gurlit et al., 2005; Hunsmann et al., 2008; Lübken et al., 1999; May, 1998; McManus et al., 1995) beam
261 setups. Further major categorizing distinguishes between the wavelength-modulation schemes like single
262 modulation frequency = direct TDLAS or dTDLAS (Ebert and Wolfrum, 1994) or double modulation
263 schemes like wavelength modulation spectroscopy WMS (Podolske and Loewenstein, 1993; Silver, 1992;
264 Silver and Hovde, 1994a; Silver and Zondlo, 2006; Vance et al., 2011; Webster et al., 2004). WMS which is
265 often used for very compact airborne sensors, provides on the first glance higher sensitivities by using lock-
266 in technologies to efficiently filter noise. This, however, sacrifices the possibility of direct physics-based
267 quality and reliability checks, since the actual measured WMS raw signal contains less spectral information



268 than a dTDLAS raw signal. This aggravates or sometimes even prevents detailed signal analysis based on
269 fundamental physical explanations. Using dTDLAS instead with a special, but less common, first principles
270 evaluation procedure (Ebert and Wolfrum, 2000; Farooq et al., 2008; Mihalcea et al., 1997; Schulz et al., 2007)
271 yields a sophisticated evaluation, characterization, and quality management and a holistic view on the
272 physical principles behind the data. This circumstance can even be used to avoid typical calibration proce-
273 dures with reference gas standards.

274

275 *Explanation of the term “calibration-free”*

276 The term “calibration-free” is often used in different communities with dissimilar meanings. To distinguish
277 one should consider how calibration is defined by metrology (JCGM 2008, 2008): “calibration (...) in a first
278 step, establishes a relation between the measured values of a quantity with measurement uncertainties pro-
279 vided by measurement standards (...), in a second step, uses this information to establish a relation for ob-
280 taining a measurement result from an indication (of the device to be calibrated)”. In other words, an in-
281 strument with a deterministic relation between indication and quantity can be calibrated, without knowing
282 the physics behind it. This particularly allows for compensating of non-linearity, offsets, drifts or response
283 changes over time as long as they are stable, predictable, or can be extrapolated. We use the term “calibra-
284 tion-free” to emphasize that HAI does not rely on such a correction process. The hygrometer described in
285 this paper has never been calibrated or adjusted to a water vapor primary standard. Of course, parameters
286 like gas pressure and temperature that are used for the calculation of the water vapor content via a first
287 principle model are measured with calibrated sensors. This is done from a practical point because a) prima-
288 ry standards for temperature and pressure are by themselves large facilities and b) the influence in the final
289 uncertainty budget doesn’t justify that approach. Calibration-free doesn’t mean that the whole setup only
290 uses primary principles. The whole idea behind traceability (JCGM 2008, 2008) is to use other sizes, higher
291 in the hierarchy of the SI units of course, to generate/analyze the target value. Metrologists name that an
292 unbroken chain of measurements. To visualize, this means that the first water vapor value delivered by the
293 HAI instrument is the final value. Everything has to be characterized in advance on such a level that the
294 first measurement value is determined within its uncertainty limits. Therefore, since there was no calibra-
295 tion, it’s termed *calibration-free*.

296 Obviously, the calibration-free approach can always be enhanced with a calibration (such as (Muecke et al.,
297 1994)) at any time (Buchholz et al., 2013b), even after a campaign if this seems advantageous, since the re-
298 quirements for a calibrated instrument are lower than for a calibration-free instrument.

299 **3.2. Non-calibrated direct TDLAS (dTDLAS)**

300 The principle of non-calibrated absolute dTDLAS is very briefly presented in the following section. More
301 detailed information regarding TDLAS is referred to in the above-mentioned literature. The sketch in Fig-
302 ure 1 shows the schematics of a dTDLAS spectrometer with two independent channels. For low light inten-
303 sities $I_0(\lambda)$ in the mW-range, the transmitted light $I(\lambda)$ can be described by the extended Lambert-Beer equa-



304 tion (Equation 1) including possible disturbances or the absorption measurement by background radiation
 305 $E(t)$ or broadband transmission losses $Tr(t)$.

306 Equation 1: $I(\lambda) = E(t) + I_0(\lambda) \cdot Tr(t) \cdot \exp[-S(T) \cdot g(\lambda - \lambda_0) \cdot N \cdot L]$

307 By applying the ideal gas law Equation 1 can be used to retrieve the H_2O volume mixing ratio c .

308 Equation 2:
$$c = -\frac{k_B \cdot T}{S(T) \cdot L \cdot p} \int \ln \left(\frac{I(v) - E(t)}{I_0(v) \cdot Tr(t)} \right) \frac{dv}{dt} dt$$

309 The *amount fraction* c is in metrological units officially specified as [mol/mol = mol absorber per mol gas]
 310 which is in the environmental community better known as “volume fraction” e.g. in units of ppmv or
 311 Vol.-%. The term $\frac{dv}{dt}$ is called the *dynamic tuning coefficient* of the used laser. It can be determined experimen-
 312 tally and is directly linked to the SI units (length) by using the Airy signal of the laser light passing through
 313 a planar, air-spaced etalon (Ebert and Wolfrum, 2000; Schlosser et al., 2002). Yet, unpublished, on-going,
 314 and long-term $\frac{dv}{dt}$ measurements for the used 1.37 μm DFB laser type over several years indicate a long-term
 315 stability of its tuning characteristics better than 1%, which is within the current uncertainties of the tuning
 316 characterisation. k_B is the *Boltzmann constant* and L is the *optical path length*. $S(T)$ is the *line strength* of the
 317 selected molecular transition (see chapter below) and therefore a physical property of the molecule to be
 318 measured. The gas *pressure* (p) and gas *temperature* (T) can be accurately acquired in a closed-path cell; the
 319 quality of the respective measurements in the open-path cell are discussed in the following chapter describ-
 320 ing the construction of the open-path sensor. Equation 2 also “explains” the term calibration-free quantita-
 321 tively as there are no other “hidden” parameters used to derive the water vapour concentration which re-
 322 quire a calibration.

323 3.3. Absorption line selection

324 Suitable absorption lines have to be selected for a specific application by several criteria (Wunderle et al.,
 325 2006) (Wagner et al., 2012). Besides a line strength maximization to ensure high sensitivity, other important
 326 parameters have to be taken into account. For atmospheric measurements, the cross sensitivity to other
 327 gases such as CO_2 needs to be minimized. This ensures a better control of the fitting process due to the few-
 328 er degrees of freedom. Similarly, the line should be isolated from other lines to simplify the retrieval of the
 329 baseline function. For the open-path measurements, it is highly important to minimize temperature de-
 330 pendence of the line strength in order to minimize the influence of gas temperature uncertainties. Lastly,
 331 sometimes the primary constraint is the availability of suitable laser diodes and additional accessories such
 332 as fibers and optic components. As the certification for airborne instruments nearly prevents improve-
 333 ments/repairs during a campaign, all components need to be very reliable. For HAL, we selected two specifi-
 334 c water lines at 2596 nm and 1370 nm in two wavelength ranges, which also had been used before
 335 (Buchholz et al., 2012, 2013b; Ebert, 2006; Ebert et al., 2004; Fahey and Gao, 2009; Hovde et al., 2001;
 336 Hunsmann et al., 2008; May, 1998; Seidel et al., 2012; Witzel et al., 2012; Wunderle et al., 2008) and for which
 337 improved spectral parameters were generated (Hunsmann et al., 2006). The 2.6 μm laser is not fiber-
 338 coupled, doesn’t have an optical isolator, is less stable in terms of temperature fluctuations and has a lower
 Page 9



339 beam quality, but accesses a factor of 20 stronger line and thus ultimately promises 20 x higher sensitivity.
340 Both lines are shown (Figure 2) as a simulation based on the HITRAN (Rothman et al., 2009) database. As-
341 suming an optical resolution of 5.10^{-4} OD, the hygrometer is expected to provide for a $1.4 \mu\text{m}$ closed-path
342 cell (assuming a 1.5 m path length) under atmospheric conditions a water vapor concentration range from
343 10 to 40 000 ppmv and for the $2.6 \mu\text{m}$ closed-path channel from 0.5 to 2000 ppmv. The lower limit will final-
344 ly be defined by the capability of minimizing and compensating the effects of parasitic H_2O offsets
345 (Buchholz and Ebert, 2014b) and their related uncertainties. For the $2.6 \mu\text{m}$ channel, the upper limit de-
346 pends strongly on the retrieval quality of the baseline. This means e.g. under lower pressure conditions
347 (<500 hPa) evaluations up to 40 000 ppmv can be performed but for high pressures the absorption line at
348 these high concentrations is saturated and so broadened that the baseline cannot be retrieved with a low
349 uncertainty. The upper limit in general, i.e. also for the $1.4 \mu\text{m}$ channels, is defined by the dew point related
350 to the instrument temperature; 40 000 ppmv is equal to 100 %RH at 28.5°C and 1013 hPa.

351 **4. HAI configuration**

352 HAI can be installed on an aircraft in several different ways and configurations. This paper focuses on the
353 installation during the first HALO (Krautstrunk and Giez, 2012) campaigns (TACTS (Engel et al., 2013) and
354 ESMVal (Schlager, 2014)) which targeted multiphase H_2O measurements. Figure 3 (right) shows the fuse-
355 lage of HALO with the two mountings belonging to HAI. In the very front is a trace gas inlet (TGI), where
356 HAI uses the second opening from the top to sample air in flight. The sampling height is approx. 25 cm
357 above the aircraft skin. Next to the TGI is the HAI open-path cell (OPc), which is a fiber-coupled, White-
358 type three-mirror configuration mounted on two pylons. The mirrors fold the laser light beam shown in the
359 middle (yellow). Both the TGI and the OPc are installed on HALO specific aperture plates. Figure 3 (left)
360 depicts the cabin installations with the golden instrument in the middle being the rack of the HAI main
361 unit. The black insulated $\frac{1}{2}$ " pipes on the right side of the rack are the inlet lines providing the air sampled
362 by the TGI to the main unit. These pipes are heated (70°C) to evaporate ice particles and droplets in the gas
363 stream at a flow of approximately 100 volume liter/min. The open-path sensor is not visible in this photo
364 since it is on the left side of the rack.

365 **4.1. HAI main unit**

366 The HAI main unit is comprised of individual modules except for some electronics of the OPc which are
367 directly mounted cabin sidewise on the OPc: preamplifier for detectors, five temperature measurement
368 converters, mirror heating controller, and two pressure sensors. Many of the modules contain innovative
369 developments, which are or will be published individually to prevent an overload of technical details in
370 this paper. The important functions/modules to understand the HAI concept are as follows:

- 371 a. Automatic line identification and spectral locking to compensate temperature and electrical influences as
372 well as drifts
- 373 b. Internal mechanism (Buchholz and Ebert, 2014b) to minimize and compensate effects from parasitic
374 absorption which usually leads to variable offset problems in spectrometers like HAI



- 375 c. Gas handling system which tempers the air to be analyzed to the temperature of the instrument and
376 therefore minimizes the risk of temperature inhomogeneity even at high gas flows as well as to provide
377 detailed information about temperature, pressure, and gas flow in and through the system
- 378 d. Several individual sensors and electronics to collect in total more than 120 system parameters about the
379 HAI system's health
- 380 e. Sequence control system for steering, controlling, and exception treatment of HAI with all its submod-
381 ules

382 4.2. HAI's closed-path cells (CPC)

383 Core parts of the HAI main unit are the extractive optical closed-path cells (Figure 4) installed in the indi-
384 vidual 1.4 μm and 2.6 μm optics modules within the HAI main unit. Both optics modules are completely
385 independent, and both cells use a new, highly compact miniature White type (White, 1976) design that folds
386 the laser beam (total approx. 1.5m) with three mirrors (approx. 7.5 cm distance). The 1.4 μm cell is an im-
387 proved fiber-coupled version of the White cell in (Kühnreich et al., 2013). Combined with a new fiber fed
388 through (Buchholz and Ebert, 2014a), it reaches a very low leakage rate of $1.9 \cdot 10^{-6}$ hPaL/s and prevents par-
389 asitic offsets due to ambient air. Three mirrors, one fiber, and one detector are the only optical parts in the
390 cell. This reduced amount of optics minimizes fringing effects efficiently down to a long-term 10^{-4} level (no
391 readjustment needed for approx. 400 flight hours within 4 years). The temperature is measured via a 3 mm²
392 accurate (0.3 K) PT100 sensor for slow temperature changes ($t_{0.5}$ approx. 2.5sec) and also with a thermocou-
393 ple (type T, 0.5 mm diameter) for faster temperature changes ($t_{0.5}$ approx. 0.5sec). Due to the above men-
394 tioned gas handling system and the thermal mass of the whole instrument (approx. 31 kg) the temperature
395 fluctuations are below 0.1 K during aircraft operation. Each cell with a volume of approx. 300 ccm is typical-
396 ly flushed during flight with a gas flow of 20 – 50 vol.liter/min per cell (depending of the installing scenario)
397 leading to a 0.7 sec flushing time using bulk flow estimation. The 2.6 μm closed-path cell is by its design
398 quite similar to the 1.4 μm . The most significant difference is the free-space beam guidance into the cell,
399 since fibers at 2.6 μm are quite critical to handle and suitable beam splitter etc. weren't available. Therefore,
400 the 2.6 μm laser, the reference cell for spectral stabilization, the beam splitters, the mirrors, and the fiber
401 coupling section for the open-path cell are enclosed in a specially designed gas tight 2.6 μm optics module
402 box. This module is internally dried by a purging cycle containing a H₂O purifier based on the same idea as
403 for removing parasitic offsets in fiber coupled hygrometer (Buchholz and Ebert, 2014b). The 2.6 μm closed-
404 path cell is directly attached to this laser module. Before reaching the cell, the laser beam is therefore "free-
405 space" guided in a water vapor free environment (typ. <0.5 ppmv) which efficiently avoids parasitic effects
406 in the beam path.

407 4.3. HAI's open-path cell (OPC)

408 HAI's open-path cell (Buchholz et al., 2013a) is – just like the closed-path cells – based on the White (White,
409 1976) principle and installed in the fuselage of HALO. Contrary to the closed-path cells, both wavelengths
410 (2.6 μm and 1.4 μm) are simultaneously coupled into the same 3 mirror cell via two independent glass fi-



411 bers. The cell (made of 2" diameter mirrors) has a mirror base distance of approximately 15 cm and is set to
412 an optical path length of 4.2 m. The optical measurement volume is located approximately 23 cm above the
413 aircraft skin. The air temperature within the open-path cell is measured via two surface-mounted platinum
414 PT100 sensors. These temperature sensors provide together with the HALO's temperature measurement
415 (Giez, 2012) and our CFD simulation (not shown here) an estimated (± 5 K) temperature in the actual meas-
416 urement volume of the open-path cell. Improved temperature field simulations will be realized in the future
417 as soon as a full CFD model of the aircraft and HAI is accessible. To prevent a dew or frost buildup on the
418 mirror surface, all three mirrors are individually heated (using approx. 20W electrical power each). This
419 raises the mirror temperature, defined by core temperature measurements of the copper mirrors, typically
420 15 – 20 K above the ambient temperature. The gas pressure measurements are done by two commercial
421 piezo pressure transmitters. Their individual ports are located on either side of the open-path cell. An in-
422 flight pressure sensor validation has been realized recently via the first optical airborne pressure measure-
423 ments. This calibration-free approach exploits the pressure dependence of the collisional broadening of the
424 water absorption line (Buchholz et al., 2014b).

425 4.4. TDLAS based multi-phase H₂O measurements

426 By simultaneously combining closed-path and open-path water measurements, HAI is the first TDLAS
427 hygrometer to allow calibration-free multi-phase water detection. The schematic of the HAI configuration is
428 shown in Figure 4. Both independent closed-path cells are connected via heated inlet lines (visible in Figure
429 3 left) to the forward facing TGI. The TGI thus samples in clouds both the *gas-phase water vapor* in conjunc-
430 tion with the *ice particles* or *H₂O droplets*. Droplets and ice particles are evaporated in the heated inlet lines,
431 so that both closed-path cells analyze the so called *total water* content, i.e. the sum of the interstitial gas
432 phase water plus the evaporated condensed phase water. This evaporation step is necessary since dTDLAS
433 is typically evaluated in a way to suppress the broad band spectra of condensed phase water and only tar-
434 gets the narrow spectral structure of water vapor. The combination of the narrow absorptions line width
435 with a narrow tuning range of diode lasers allows this discrimination of gas-path water vapor from the
436 broad spectra of ice or liquid water. The open-path cell, which is directly located on the fuselage of HALO,
437 however, measures the pure interstitial gas-phase water vapor of the air which flows through the cell. By
438 combining the total water and the gas phase water measurement, i.e. closed-path and open path signals, it
439 is possible to derive from the difference of both HAI signals the pure condensed water phase, i.e. the
440 ice/droplet phase. To our knowledge, HAI is the first airborne instrument that can measure all water phases
441 with the same detection principle, the same evaluation strategy, and with two channels, each spectroscopi-
442 cally and temporally linked by one single laser. When independent devices have been used previously to
443 measure these water products, even with similar TDLAS instruments like in (Vance et al., 2015), this always
444 led to the discussion on how much of the deviations are caused by atmospheric effects and how many are
445 linked to discrepancies between the participating instruments caused by different characteristics, response
446 times or nonlinearities of the individual instruments. Indeed, the calibration or even validation of all other
447 open-path hygrometers cited above is based on laboratory measurement or comparisons with other hy-



448 grometers with different properties which makes it nearly impossible to justify more than statistical
449 (=averaged) statements. HAI avoids these discussions by various self-validations.

450 **4.5. Self-validation**

451 The new self-validating capabilities are a consequence of the unique 2x2 multi-channel configuration, which
452 enables six individual validation pathways, as illustrated in Figure 5. Under clear-sky (= cloud-free) condi-
453 tions, the independent open-path and closed-path measurements should each deliver the same value. Im-
454 portant to note is that both the 1.4 μm and the 2.6 μm spectrometer channels are evaluated without com-
455 mon parameters in calibration-free first principles mode. This means in detail: two different lasers, two
456 different absorption paths, two different absorption lines, different line parameters, different electronics etc.
457 Nevertheless, both spectrometer channels have to agree within their uncertainty if the first principle evalua-
458 tion is applicable. Due to the large overlapping H₂O concentration range of approximately 50 to 5000 ppmv,
459 all disturbances can be clearly identified as long as they affect both spectrometers differently. Outside of
460 clouds (clear-sky) – i.e. in ice particle/droplet-free air – all four channels spectrometer channels have to
461 agree. This in particular allows to validate (or even if necessary to calibrate) the closed-path cells in a labor-
462 atory environment and to use them as an airborne transfer standard to validate or even calibrate in turn the
463 open-path sensor in flight. This is a unique property of HAI, since each open- and closed-path spectrometer
464 are coupled by one single laser and all four spectrometers are employing the same evaluation procedure.
465 Hence, HAI is called a 2x2 spectrometer.

466 **5. Results**

467 **5.1. Signal assessment**

468 Figure 6 shows - at the same instant of time - all seven raw optical signals from HAI's measurement chan-
469 nels at approx. 15000 ppmv and 900 hPa. For visualization, the signals of each laser are scaled to the same
470 peak maximum, since transmission changes are irrelevant according to the equation for concentration re-
471 trieval (Equation 2). The time axis (240 Hz laser repetition rate) is already converted to the wavelength axis
472 using the dynamic tuning rate. The triangular diode laser current modulation yields to a triangular modula-
473 tion of the beam intensity and a similar shape in the wavelength. The tuning range of the 2.6 μm laser is set
474 to be broader in order to allow the evaluation of high absorbance spectra when the peak absorption is in
475 saturation in the absorption line centre. In this case, the Lorenz wings carry the concentration information.
476 The absorbance of the 1.4 μm open-path signal (purple) is higher than the one from the closed-path cell, due
477 to the threefold longer optical path length in the open-path cell. The 1.4 μm reference cell signal (blue) is
478 used for spectral stabilization and acquired from a low pressure (approx. 20 hPa) fibre coupled reference
479 cell. The signal for retrieving and compensating parasitic absorption is shown in green and the associated
480 evaluation is described in (Buchholz and Ebert, 2014b). Accordingly, the three 2.6 μm signals are shown. The
481 parasitic absorption compensation of the 2.6 μm system is due to the "free-space" signal in the sealed laser



482 module (see description above) at least as important as the one for the 1.4 μm spectrometer. This compensa-
483 tion treatment is done using an ultra-low pressure (approx. 0.5 hPa) reference cell which provides infor-
484 mation for both, the spectral stabilization and the parasitic absorption correction. The latter approach is
485 described as “two pressure separation method” in (Buchholz and Ebert, 2014b).

486 Figure 7 and Figure 8 show four typical absorption signals in flight with a pre-average of 50 raw measure-
487 ments done at 240 Hz. This leads to 4.8 measurements per second with a time resolution of 70 ms for each
488 reading while only approx. 1/6 of the whole spectral scan is necessary for the evaluation. Figure 7 allows the
489 simultaneous comparison of both closed-path cells. Gas pressure and temperature are slightly different due
490 to the different piping and installation placement inside of HAI. Both H_2O concentrations agree ($\Delta = 1.6\%$)
491 within the combined uncertainties (7.9%) of both channels. Each graph in Figure 7 shows in the top the
492 measured data (green dots) with the fitted Voigt profile (black line). The measurement data are shown as
493 absorbance ($\text{ODe} = -\ln(I/I_0)$) values, i.e. the detector (I) signal divided by the so called “base line” (I_0). The
494 baseline resembles the absorption spectrum in the absence of the molecular target absorption. It is retrieved
495 from the raw spectrum (I) by applying a synchronous polynomial fit of the baseline and a Voigt profile for
496 the absorption line. The residuals between measured data and the model function are depicted below. The
497 remaining structures visible in the residual are optical interference fringes, caused by light scattered from
498 imperfect mirrors, the fiber surface, or the detector arrangement. The repetition frequency of a fringe can be
499 linked to the optical distances between the interfering surfaces. So far, these baseline structures as well as
500 the cell alignment remained stable over the past years. The mirrors never required cleaning during the last
501 four years. Of course, the entire fringe structure can be phase shifted by temperature. However, compared
502 to WMS systems, where fringe levels have to be reduced down to the 10^{-6} OD level to achieve high sensitivi-
503 ties, our calibration-free dTDLAS evaluation is designed to require a stable baseline on the 10^{-4} OD level,
504 which makes it inherently robust. In other words, dTDLAS systems like HAI are usually not as sensitive to
505 misalignments, dirt, and optical structures as WMS systems. On the other hand, they require higher absorb-
506 ance for the calibration-free approach.

507 Figure 8 shows a simultaneous comparison between the open-path and the closed-path channel. The out-
508 side gas temperature in the open-path cell is approx. 52 K lower than in the closed-path cell. The gas pres-
509 sure in the closed-path cell, on the other hand, is much higher than in the open-path cell, due to the ramp
510 pressure guiding the air through the TGI and the piping. The measured water vapour concentrations are
511 slightly shifted in time due to the gas transport and the sampling delay in the pipes. The 1σ residual is a
512 factor of six higher in the open-path than in the closed-path sensor. This mainly results from the high wind
513 speed through the open-path cell (approx. 800 km/h). It is important to mention that for diode laser instru-
514 ments a change of gas temperature, pressure, and concentration over a large range can commonly cause
515 large systematic offsets, which frequently would require at a least three dimensional calibration surface
516 (depending on pressure, temperature, concentration) or to the integration of complex assumptions (Duffin
517 et al., 2007; Goldenstein et al., 2014; Rieker et al., 2009) to correct the data via a simulation model. WMS
518 closed-path systems usually avoid this problem by always keeping temperature and pressure as close and
519 constant as possible to the calibrated level which is obviously not a viable approach for an open-path sys-
520 tem.



521 5.2. Precision

522 One common figure of merit to quantify the short term optical precision of a spectrometer is the 1σ noise
523 level in the residuum. The idea is based on the assumption that the residual is governed by random noise
524 which limits the precision of the system. The Signal-to-Noise Ratio (SNR) is then defined by the *signal* as the
525 OD_{peak} value and the *noise* by the statistical standard deviation of the residual and thus equals to OD_{noise} .
526 This definition yields for the 1.4 μm /2.6 μm closed-path cells at 4.8 Hz time resolution a SNR of 54 respec-
527 tively to an SNR of 204. The corresponding precision is then $100/54 \text{ ppmv} = 1.9 \text{ ppmv}$ (1.4 μm) respectively
528 $100/204 \text{ ppmv} = 0.49 \text{ ppmv}$ (2.6 μm). This determination is quite consistent with Figure 8 where the preci-
529 sion of the 1.4 μm closed-path can be estimated to 1.3 ppmv in the same way. However, as the fringe struc-
530 ture of the closed-path cell is quite stable it is better to determine the instrument precision via the Allan
531 variance (Allan, 1966). Figure 9 shows the Allan plot for both closed-path cells. The measurement was done
532 at 255 ppmv by measuring gas from a big vessel. Under these conditions, the precision at 4.8 Hz is
533 0.22 ppmv (for the 1.4 μm closed-path cell) respectively 0.065 ppmv (2.6 μm closed-path cell). Both values
534 are approximately a factor of 8 lower than the one derived from the single scan analysis, which confirms the
535 stability thesis of fringes. Vice versa we can derive an actual (= unstable, random) 1σ residual OD noise
536 level of $2.3\text{E-}5$ for the 1.4 μm closed-path and $1.7\text{E-}4$ ppmv for the 2.6 μm closed-path cell. The best preci-
537 sion is achieved at 3.9 Hz (0.18 ppmv) for the 1.4 μm cell and at 13 Hz (0.055 ppmv) for the 2.6 μm cell,
538 normalizing this with respect to time resolution and optical path length yields a 1σ precision of 187
539 $\text{ppbv}\cdot\text{m}\cdot\text{Hz}^{-1/2}$ (1.4 μm) and 31 $\text{ppbv}\cdot\text{m}\cdot\text{Hz}^{-1/2}$ (2.6 μm).
540 Comparing that precision ratio of 6 between the 1.4 μm and the 2.6 μm to the ratio in line strength of 20 (see
541 line selection chapter 3.3) confirms the statement mentioned above that drawbacks of the longer wave-
542 length technology significantly constrain the practically achievable maximum gain.
543 For the open-path sensor, we have not yet been able to calculate an Allan variance so far, since we haven't
544 acquired a data set in flight where atmospheric water was constant enough not to dominate the Allan vari-
545 ance via natural H₂O fluctuations. However, using the short term single spectrum evaluation method in
546 Figure 8, one can calculate a SNR of 145, which yields a precision of 2.1 ppmv (= $4.6 \text{ ppmv}\cdot\text{m}\cdot\text{Hz}^{-1/2}$).

547 5.3. Uncertainty consideration

548 One of the major benefits of the dTDLAS evaluation done with HAI is the high level of control over the
549 fitting/evaluation process. In particular, when it is combined with the complete storage of all the raw data,
550 this allows for a dedicated and highly flexible post-flight analysis or post-flight processing. Raw data stor-
551 age for HAI not only covers all raw spectra but also approximately 120 measured parameters depicting the
552 complete status of the HAI instrument. This "housekeeping data" for example, encompasses 15 tempera-
553 ture measurements that allow for diagnostic statements e.g. about temperature inhomogeneity, electronic
554 drift, or sensor malfunctions. Housekeeping data like these facilitate assignments of a measurement uncer-
555 tainty closer to the one in a metrological sense (Joint Committee for Guides in Metrology (JCGM), 2008). If
556 measurements are done in harsh environments or under rapidly changing conditions, typical concepts of
557 metrological uncertainty assessments fall short since most of their concepts are developed for laboratory



558 applications under quasi-static conditions. But even in this case the housekeeping parameters provide in-
559 formation for a trustful uncertainty consideration. The uncertainty calculations below are based on a physi-
560 cal model (Equation 2) and are performed with an approach independent from the actual measurement.
561 Depending on the individual science community uncertainties, errors, reproducibility, or misreading are
562 often determined by comparing the readings of an instrument to reference instrument. This is contrary to a
563 metrological uncertainty and furthermore a non-independent approach; we call that therefore simply *devia-*
564 *tion, standard deviation* etc.

565 According to the Equation 2 for retrieving the final concentration the individual contributions to the total
566 uncertainty budget can be assessed as followed for both closed-path cells. The optical path length was pri-
567 marily determined with a Zemax based ray tracing simulation. In addition, it was calculated by the me-
568 chanical mirror distance and compared to a test measurement with a known amount of CH₄ gas in the cell.
569 These measurements lead to an uncertainty of the optical-path length of 15 mm (1.1%). The uncertainty for
570 the used H₂O absorption line strength is 3.5% [44]. The temperature sensors (PT100 and thermocouple type
571 E as described above) are calibrated against metrological transfer standards (Rosemount platinum re-
572 sistance thermometer type 162CE (PRT-25), uncertainty 1.5 mK). Due to the well-known fact that tempera-
573 ture measurements in moving gases suffer from many issues, we use a conservative estimation of 1K (0.3%).
574 The manufacture of the pressure sensors (Omega PAA33X) advertises a resolution of 0.02 hPa and a long-
575 term accuracy of 0.5 hPa. We use 1 hPa as a conservative uncertainty estimation. A general statement for the
576 laser tuning uncertainty is difficult in a metrological sense, since it depends on local effects in the spectra,
577 pressure range, concentration level and number of absorption lines fitted. From our experience, we assume
578 that deviations related to the fitting process in total (tuning + fit process) are in the range of below 1.5%. As
579 a conservative approximation we use 2% for the fit and 1% for the tuning. This yields to a total uncertainty
580 of 4.3%. for the 1.4 μm closed-path cell.

581 The largest relative influence to this total uncertainty budget results from the line strength (66%), followed
582 by the fitting uncertainty (21%), as well as the optical path length (7%). Additionally, the offset uncertainty
583 is defined in a calibration-free dTDLAS system by the capability of minimizing and determining parasitic
584 effects. It is ±3 ppmv for the 1.4 μm closed-path cell of HAI, which uses the same parasitic prevention
585 treatment as SEALDH-II (Buchholz and Ebert, 2014b). Thus, the total uncertainty of the 1.4 μm closed-path
586 system is 4.3% ±3 ppmv. Similar considerations lead to an uncertainty of 5.9% ±0.4 ppmv for the 2.6 μm
587 closed-path cell.

588 Related to the open-path cell, the statement is more difficult. First of all, a full CFD model of the boundary
589 layer around HALO is currently missing, which would allow a retrieval of the gas temperature in the open-
590 path cell. The first CFD test runs of HAI's open-path sensor and its immediate surroundings have been
591 realized (A. Afchine (FZJ), published in (Klostermann, 2011)), and led to a first temperature uncertainty
592 estimate of ±7 K. The full CFD model could also provide pressure field calculations. However, in this case,
593 we developed a method on how to retrieve the pressure directly from the dTDLAS signal (Buchholz et al.,
594 2014b) and use that for a validation of the built-in micromechanical pressure sensor. The pressure depend-
595 ent uncertainty is in the range of 3-5%. The uncertainty of the fitting process reveals a much higher com-
596 plexity. It depends on all impacts on the spectral signal itself such as: background radiation on the detector,



597 misalignment due to the distortion of the HALO fuselage, forming of an ice layer on the mirrors, high opti-
598 cal dense cloud transects, eddies around the aircraft etc. From all the data gathered and compared during
599 the HALO missions TACTS and ESMVal, we couldn't find any deviation larger than $\pm 5\%$ in clear sky condi-
600 tions between the open-path and the closed-path sensor which couldn't be clearly linked to explainable
601 effects. Besides of the availability of an entire CFD model in the future, HAI will be validated by sampling
602 the pure water vapor gas-phase (backward measurement) with its closed-path cells in future campaigns.
603 These datasets will sustainably prove if the $\pm 5\%$ deviation is valid under all conditions, since then all four
604 channels of HAI (Figure 5) would permanently measure the same atmospheric value. Compared to the de-
605 viations, revealed in the AQUAVit (Fahey et al., 2014) intercomparison of state of the art, airborne hygrome-
606 ter in 2007, this 5% is fourfold smaller than the span (20%) of those instruments there. Additionally, one has
607 to keep in mind that this comparison was done under quasi-static laboratory conditions. Therefore, this in-
608 flight 5% deviation between the open-path and the closed-path sensor shows the great performance of HAI,
609 even if a general metrological uncertainty is difficult to be given yet at this time.

610 **5.4. First airborne measurements with HAI on the HALO aircraft**

611 Figure 10 shows typical HAI measurements during the first HALO science mission "TACTS/ESMVal". The
612 chosen flight profile shows 15 min of a slow ascent from the lower to the upper troposphere. Depicted in
613 Figure 10 are: the H_2O concentration measured with the $1.4\ \mu\text{m}$ CPc (black), $1.4\ \mu\text{m}$ OPc (magenta), and
614 $2.6\ \mu\text{m}$ CPc (red) channel of HAI (left axis) as well as the ambient gas pressure (right y-axis, in blue), which
615 is directly connected to the flight level (height). Other instruments indicated that HALO flew in the early
616 part of the flight (left) in clear sky conditions (no clouds). All Figure 10 data were plotted with 1 Hz tem-
617 poral resolution. With increasing height, the H_2O concentration declines about 2.5 magnitudes from approx-
618 imately 2000 ppmv to 75 ppmv, in combination with simultaneous relative pressure variation from approx.
619 175 to 450 hPa ($\Delta p=275$ hPa). The H_2O concentrations, measured with HAI's two independent closed-path
620 spectrometer channels, fit nicely to each other and show only a small average relative deviation of 1.9%
621 (bottom graph in red), which is entirely covered by the uncertainty range of each spectrometer (4.3% resp.
622 5.9%). This result is consistent with other measurements, where the $2.6\ \mu\text{m}$ path was persistently on aver-
623 age approx. 2% higher than the $1.4\ \mu\text{m}$ channel. This could be easily explained with the $2.6\ \mu\text{m}$ line strength
624 from the HITRAN database being 2% too small. The 1.9% deviation also needs to be related to the fact that
625 both hygrometer channels are evaluated completely independently, without any calibration of the instru-
626 ment and most importantly under real-world flight conditions. Despite these demanding conditions HAI's
627 two closed-path channels generate a relative deviation which is just 1/10 of the above mentioned 20% in
628 AquaVIT (Fahey et al., 2014), which demonstrates the excellent accuracy of the HAI spectrometers.
629 The purple signal also depicted in Figure 10 shows the measurement of the $1.4\ \mu\text{m}$ open-path sensor
630 ($1.4\ \mu\text{m}$ OPc). Compared to the $1.4\ \mu\text{m}$ closed-path cell ($1.4\ \mu\text{m}$ CPc), the $1.4\ \mu\text{m}$ OPc shows a relative devia-
631 tion of $\pm 5\%$ peak-to-peak or 2% on average. This performance of the $1.4\ \mu\text{m}$ OPc is to be compared with
632 previously described airborne hygrometer which resemble the current state of the art. However, it has to be
633 noted that a huge number of airborne hygrometers with an extreme diversity in sensing principles and



634 specific performances have been published and described, so that a general overall statement about the
635 “state of the art” is very difficult to make. In addition, there is a very large variation in sensor accuracy and
636 the performance figures stated are sometime misleading and contradictory to the results of the few rare
637 large scale intercomparisons like AquaVIT. However, a short incomprehensive review on the performance
638 of previous open-path instruments should be given here:

639 a) A calibrated, 1 m direct absorption, open-path sensor at $1.4\mu\text{m}$ was developed in a feasibility study for
640 the Strato 2C research aircraft and described to cover a concentration range of 2-2000 ppmv with 100 ppb
641 precision at 1 Hz. It was claimed to have an accuracy of 5% , but this hygrometer never flew (Roths and
642 Busen, 1996).

643 b) A calibrated open-path sensor with an optical path length of 375 cm, folded in a Herriot cell, and a time
644 resolution of 25 Hz gave a precision of 80 ppbv. This instrument is designed for the American HAIPER
645 (Anon, n.d.) aircraft, a Gulfstream 550 like the HALO aircraft. To our knowledge this is the only open-
646 path hygrometer which was frequently installed and used during the last years on an aircraft. Typical
647 deviations to other instruments were in the range between 2% and 10% (Zondlo et al., 2010).

648 c) Another calibrated, Herriot cell based open-path hygrometer with a total path length of 11 m, a meas-
649 urement frequency up to 10 Hz and a precision of 50 ppbv at 0.5 Hz. This instrument claims to have an
650 uncertainty of 5% to 10% (May, 1998). However, to the best of our knowledge, except of a few test
651 flights, no further flight was nor published or performed.

652 In summary, HAI’s 2% deviation appears to be much better than typical statements in publications.

653 To further evaluate the performance of HAI’s open-path channels we further discuss the TACTS data. The
654 dark purple line shows the data after smoothing them with a 60 second sliding window algorithm. Quite
655 interesting are the two dents at 13:41 and 13:44 in the relative deviation, which means the closed-path
656 measurement was higher than the open-path measurement. Both of them happened after the water vapour
657 concentration dropped sharply. Hence, the dents might be explained by desorption processes inside of the
658 TGI, its piping and the measurement cell. This idea is backed by the $1.4\mu\text{m}$ to $2.6\mu\text{m}$ closed-path compari-
659 son (red). The same behaviour is also visible at 13:44, but here the $2.6\mu\text{m}$ close path cell added less desorp-
660 tion water to the gas steam than the $1.4\mu\text{m}$ one. Another influence leading to that deviation could be a
661 temperature measurement on HALO affected by fast changes of humidity. The total temperature influence
662 in Equation 2 is at this temperature and pressure approximately 0.6%/K caused by the temperature influ-
663 ence via the ideal gas law, the line strength temperature dependence and the Gaussian width. This brief
664 insight in a detailed data discussion demonstrates the unique opportunities offered by HAI, which allow a
665 deep analysis to identify and eventually classify different measurement sections of a flight in order to dis-
666 tinguish instrumental artefacts from real atmospheric situations.

667 On the second part of the flight shown in figure Figure 10 , the aircraft passes through ice clouds (Cirrus,
668 temperature $< -40\text{ }^\circ\text{C}$). The evaporation of the ice crystals captured by the gas inlet leads to a clear en-
669 hancement of the amount of water vapor in the closed-path cells. The relative comparison shows a $\pm 5\%$
670 noisy structure, which is caused by the low time resolution of just 1 Hz. H_2O gradients in this particular
671 part of the flight are in the range of several 1000 ppmv/s. Due to SSD space limitations in the first campaign,
672 only parts of the flights where sampled with the highest time resolution of 240 Hz, in the other parts the



673 data where online pre-averaged. Like in the clear sky region, the average deviation between both closed-
674 path cells during cirrus cloud transects remains at 2%. To further check the accuracy of the open-path chan-
675 nel, we use two methods: The first is based on the physical argument that the gas-phase measurement al-
676 ways has to be lower than the total water measurement, which consists of gas-phase plus evaporated
677 ice/liquid phase. This requirement is entirely fulfilled. The second check compares the absolute gas-phase
678 measurement with the saturation mixing ratio (SMR). In case of a fully equilibrated cloud, the gas-phase
679 has to be saturated at temperature T , meaning that the relative humidity is $rH = 100\%$, from which we can
680 also derive a SMR with the help of the water vapour partial pressure curve. This is a weaker check, since it
681 is a well-known fact that super saturation can occur during strong air updrafts.

682 The transition region at the fringe of the cloud is also very interesting, where the closed-path cell sees an
683 enhancement while being still below the SMR. This means that the fringe of the cloud was not saturated but
684 had sublimating ice particles in it.

685 These first detailed close-ups in HAIs multi-phase measurements show the potential to investigate many
686 interesting questions in the following campaigns focusing on Cirrus clouds which are strongly linked to a
687 very reliable accuracy study for the open-path cell in clouds. To really investigate and fully understand all
688 effects, HAI needs more data in Cirrus, mixed-phase and other clouds in a multi-phase configuration as
689 well as a validation campaign in which closed- and open-path cells measure the pure gas-phase via a back-
690 ward measurement. The latter is necessary to distinguish between sampling-effects and optical/spectral-
691 effects in and outside of clouds. This knowledge, especially in combination with the mentioned CFD model,
692 will then allow to reevaluate HAI's raw data which are always saved during flights and extent statements
693 even for this short cirrus transect.

694 **6. Conclusion and outlook**

695 The novel *Hygrometer for Atmospheric Investigation*, HAI, realizes in a unique concept a simultaneous gas-
696 phase and total water measurement. Based on calibration-free direct tuneable diode laser absorption spec-
697 troscopy, HAI allows accurate, precise (0.065 ppmv at 4.8 Hz, channel depended) and very fast (up to
698 240 Hz) measurements with a metrologically defined uncertainty (4.3%, channel dependent). HAI contains
699 four measurement channels, grouped as two completely independent dual-channel spectrometers, one at
700 1.4 μm and one at 2.6 μm to cover the entire H_2O concentration range of the atmosphere. Each spectrometer
701 feeds light in a wavelength-individual extractive, closed-path cell with an optical absorption path length of
702 1.5 m for total water measurements. Additionally, both spectrometers couple their light in a common open-
703 path cell (optical path of 4.8 m) located outside of the aircraft fuselage, for a sampling-free and contactless
704 determination of the gas-phase water content. These four spectroscopic channels plus three additional sup-
705plementary spectroscopic channels allow multiple self-validation strategies inside and outside of clouds
706 and therefore solve the current lack of an integrated approach to validate open-path sensors in flight. HAI's
707 complex control software minimizes maintenance at ground and ensures almost entirely autonomous oper-
708ation. In addition, instrument health is permanently supervised by permanent storage of a set of more than



709 120 housekeeping data. This enables a novel, holistic quality management and a sophisticated signal cross
710 check, which guarantees a high trust level of the final H₂O values.

711 HAI was operated for the first time during the TACTS/ESMVal flight campaign for more than 120 operation
712 hours without any malfunction. The entirely independent, never calibrated first principles evaluation of the
713 closed-path spectrometer channels reduced in-flight deviations to only 1.9% over a large concentration
714 (75 to 2000 ppmv) and pressure range (175 to 450 hPa). The deviation between the open-path and the
715 closed-path measurements in the same flight segment was just 2%. Despite measuring with a single evaluation
716 concept, over a very broad range of conditions (i.e. temperatures (-70°C to 30°C), gas speeds (cm/s vs
717 100 m/s), optical disturbances (no background light vs sunlight, clean mirrors vs. dirty scratched mirrors
718 outside), HAI provided a high trust level of the data over extensive science missions. Laboratory evalua-
719 tions demonstrated the lowest achievable precision of 0.18 ppmv (at 3.8 Hz) for the 1.4 μm closed-path cell
720 and 0.055 ppmv (at 13 Hz) for the 2.6 μm closed-path cell.

721 In conclusion, HAI proved during its first deployment a novel, highly complex and demanding set of capa-
722 bilities. This will enable in the future a much more accurate and stringent evaluation of atmospheric multi-
723 phase water vapor data inside and outside of clouds and foster in further HALO missions the investigation
724 of new scientific questions in the atmospheric water cycle. HAI can serve in the future as a major, powerful
725 tool for cutting-edge atmospheric water vapor measurements.

726

727 *Acknowledgements:*

728 *Parts of this work were funded by Deutsche Forschungsgemeinschaft, DFG, via FKZ EBE 235/3 and SCHI 872/2.*
729 *Numerous metrological questions were partially co-funded via the EMRP/EMPIR projects METEOMET-1 and ME-*
730 *TEOMET-2. The EMRP/EMPIR is jointly funded by the EMRP/EMPIR participating countries within EURAMET*
731 *and the European Union. The authors wish to thank M. Riese (Forschungszentrum Jülich) for the strong, continued*
732 *support of the project; Mark Zondlo (University Princeton) for sharing his broad knowledge about atmospheric water*
733 *vapor measurements; A. Engel and H. Bönisch (Goethe Universität Frankfurt) for their coordination of the TACTS*
734 *campaign; H. Schlager for organising the ESMVal campaign. A. Giez, M. Zöger, V. Dreiling, K. Witte and A. Mini-*
735 *kin, representatives of the Deutsche Luft und Raumfahrtzentrum Oberpfaffenhofen, for providing the HALO avionic*
736 *data.*

737

738

739

740


 741 **7. References**

- 742 Allan, D. W.: Statistics of atomic frequency standards, *Proceedings of the IEEE*, 54(2), 221–230,
 743 doi:10.1109/PROC.1966.4634, 1966.
- 744 Anon: FAAM Aircraft Water Vapour Measurements, Change, 2010, 2010.
- 745 Anon: High Altitude and Long range research aircraft, <http://www.halo.dlr.de/> (last accessed: May 2014),
 746 2014.
- 747 Anon: UCAR/NCAR - Earth Observing Laboratory, 2005-present. NSF/NCAR GV HIAPER Aircraft,
 748 <http://dx.doi.org/10.5065/D6DR2S>, n.d.
- 749 Brewer, P. J., Milton, M. J., Harris, P. M., Bell, S. a, Stevens, M., Scace, G., Abe, H. and Mackrodt, P.: Euramet
 750 1002: International comparability in measurements of trace water vapour, in *National Physical Laboratory*
 751 *Report AS 59.*, 2011.
- 752 Buchholz, B. and Ebert, V.: Compact, compression-free, displaceable, and resealable vacuum feedthrough
 753 with built-in strain relief for sensitive components such as optical fibers, *Review of Scientific Instruments*,
 754 85(5), 055109, doi:10.1063/1.4872076, 2014a.
- 755 Buchholz, B. and Ebert, V.: Offsets in fiber-coupled diode laser hygrometers caused by parasitic absorption
 756 effects and their prevention, *Measurement Science and Technology*, 25(7), 075501, doi:10.1088/0957-
 757 0233/25/7/075501, 2014b.
- 758 Buchholz, B., Böse, N., Wagner, S. and Ebert, V.: Entwicklung eines rückführbaren, selbstkalibrierenden,
 759 absoluten TDLAS-Hygrometers in kompakter 19" Bauweise, in *AMA-Science*, 16. GMA/ITG-Fachtagung
 760 *Sensoren und Messsysteme 2012*, pp. 315–323., 2012.
- 761 Buchholz, B., Afchine, A., Klein, A., Barthel, J., Klostermann, T., Kallweit, S., Krämer, M., Schiller, C. and
 762 Ebert, V.: Eine neue, fasergekoppelte offene White-Zelle für die „ open-path “-Gasanalyse auf
 763 Forschungsflugzeugen, in *DGAO Proceedings*. [online] Available from: http://www.dgaoproceedings.de/download/114/114_b35.pdf, 2013a.
- 765 Buchholz, B., Kühnreich, B., Smit, H. G. J. and Ebert, V.: Validation of an extractive, airborne, compact TDL
 766 spectrometer for atmospheric humidity sensing by blind intercomparison, *Applied Physics B*, 110(2), 249–
 767 262, doi:10.1007/s00340-012-5143-1, 2013b.
- 768 Buchholz, B., Böse, N. and Ebert, V.: Absolute validation of a diode laser hygrometer via intercomparison
 769 with the German national primary water vapor standard, *Applied Physics B*, 116(4), 883–899,
 770 doi:10.1007/s00340-014-5775-4, 2014a.
- 771 Buchholz, B., Afchine, A. and Ebert, V.: Rapid, optical measurement of the atmospheric pressure on a fast
 772 research aircraft using open-path TDLAS, *Atmospheric Measurement Techniques*, 7, 3653–3666,
 773 doi:10.5194/amt-7-3653-2014, 2014b.
- 774 Buck, A.: The Lyman-alpha absorption hygrometer, in *Moisture and Humidity Symposium Washington*,
 775 DC, Research Triangle Park, NC, pp. 411–436., 1985.
- 776 Busen, R. and Buck, A. L.: A High-Performance Hygrometer for Aircraft Use: Description, Installation, and
 777 Flight Data, *Journal of Atmospheric and Oceanic Technology*, 12, 73–84, doi:10.1175/1520-
 778 0426(1995)012<0073:AHPHFA>2.0.CO;2, 1995.
- 779 Cerni, T. A.: An Infrared Hygrometer for Atmospheric Research and Routine Monitoring, *Journal of*
 780 *Atmospheric and Oceanic Technology*, 11, 445–462, doi:10.1175/1520-
 781 0426(1994)011<0445:AIHFAR>2.0.CO;2, 1994.
- 782 Desjardins, R., MacPherson, J., Schuepp, P. and Karanja, F.: An evaluation of aircraft flux measurements of
 783 CO₂, water vapor and sensible heat, *Boundary-Layer Meteorology*, 47(1), 55–69, doi:10.1007/BF00122322,
 784 1989.
- 785 Diskin, G. S., Podolske, J. R., Sachse, G. W. and Slate, T. A.: Open-path airborne tunable diode laser
 786 hygrometer, in *Proc. SPIE 4817, Diode Lasers and Applications in Atmospheric Sensing*, vol. 4817, pp. 196–
 787 204., 2002.



- 788 Duffin, K., McGettrick, A. J., Johnstone, W., Stewart, G. and Moodie, D. G.: Tunable diode-laser
789 spectroscopy with wavelength modulation: A calibration-free approach to the recovery of absolute gas
790 absorption line shapes, *Journal of Lightwave Technology*, 25(10), 3114–3125, doi:10.1109/JLT.2007.904937,
791 2007.
- 792 Durry, G., Amarouche, N., Joly, L. and Liu, X.: Laser diode spectroscopy of H₂O at 2.63 μm for atmospheric
793 applications, *Applied Physics B*, 90(3-4), 573–580, doi:10.1007/s00340-007-2884-3, 2008.
- 794 Ebert, V.: In situ absorption spectrometers using near-IR diode lasers and rugged multi-path-optics for
795 environmental field measurements, *Laser Applications to Chemical, Security and Environmental Analysis*,
796 *Technical Digest (Optical Society of America)*, paper WB1, doi:10.1364/LACSEA.2006.WB1, 2006.
- 797 Ebert, V. and Wolfrum, J.: Absorption spectroscopy, in *OPTICAL MEASUREMENTS-Techniques and*
798 *Applications*, ed. F. Mayinger, pp. 273–312, Springer., 1994.
- 799 Ebert, V. and Wolfrum, J.: Absorption spectroscopy, in *Optical Measurements - Techniques and*
800 *Applications (Heat and Mass Transfer)*, edited by F. Mayinger and O. Feldmann, pp. 273–312, Springer
801 Heidelberg, München., 2000.
- 802 Ebert, V., Fernholz, T. and Pitz, H.: In-situ monitoring of water vapor and gas temperature in a coal fired
803 power-plant using near-infrared diode lasers, in *Laser Applications to Chemical and Environmental*
804 *Analysis*, vol. 26, pp. 77–79, OSA Technical Digest (Optical Society of America, Washington DC). [online]
805 Available from: <http://www.opticsinfobase.org/abstract.cfm?id=142068> (Accessed 25 November 2013a),
806 2000.
- 807 Ebert, V., Fernholz, T. and Pitz, H.: In-situ monitoring of water vapour and gas temperature in a coal fired
808 power-plant using near-infrared diode lasers, in *Laser Applications to Chemical and Environmental*
809 *Analysis*, pp. 4–6, Optical Society of America. [online] Available from:
810 <http://www.opticsinfobase.org/abstract.cfm?id=142068> (Accessed 15 February 2012b), 2000.
- 811 Ebert, V., Teichert, H., Giesemann, C., Saathoff, H. and Schurath, U.: Fibre-Coupled In-situ Laser
812 Absorption Spectrometer for the Selective Detection of Water Vapour Traces down to the ppb-Level, in *tm -*
813 *Technisches Messen*, vol. 72, pp. 23–30, Düsseldorf., 2004.
- 814 Engel, A., Boenisch, H. and & TACTS-Team: An overview on the TACTS mission using the new German
815 research aircraft HALO in summer 2012, EGU General Assembly, 15(EGU2013-9191) [online] Available
816 from: <http://adsabs.harvard.edu/abs/2013EGUGA..15.9191E> (Accessed 1 August 2013), 2013.
- 817 Fahey, D. and Gao, R.: Summary of the AquaVIT Water Vapor Intercomparison: Static Experiments, source:
818 https://aquavit.icg.kfa-juelich.de/WhitePaper/AquaVITWhitePaper_Final_23Oct2009_6MB.pdf (last
819 accessed: May 2014), 2009.
- 820 Fahey, D. W., Saathoff, H., Schiller, C., Ebert, V., Peter, T., Amarouche, N., Avallone, L. M., Bauer, R.,
821 Christensen, L. E., Durry, G., Dyroff, C., Herman, R., Hunsmann, S., Khaykin, S., Mackrodt, P., Smith, J. B.,
822 Spelten, N., Troy, R. F., Wagner, S. and Wienhold, F. G.: The AquaVIT-1 intercomparison of atmospheric
823 water vapor measurement techniques, *Atmospheric Measurement Techniques*, 7, 3159–3251,
824 doi:10.5194/amt-7-3159-2014, 2014.
- 825 Farooq, A., Jeffries, J. and Hanson, R.: In situ combustion measurements of H₂O and temperature near 2.5
826 μm using tunable diode laser absorption, *Measurement Science and Technology*, 19(7), 075604,
827 doi:10.1088/0957-0233/19/7/075604, 2008.
- 828 Friehe, C., Grossman, R. and Pann, Y.: Calibration of an airborne Lyman-alpha hygrometer and
829 measurement of water vapor flux using a thermoelectric hygrometer, *Journal of Atmospheric and Oceanic*
830 *Technology*, 3(2), 299–304 [online] Available from: [http://journals.ametsoc.org/doi/abs/10.1175/1520-](http://journals.ametsoc.org/doi/abs/10.1175/1520-0426(1986)003<0299:COAALA>2.0.CO;2)
831 [0426\(1986\)003<0299:COAALA>2.0.CO;2](http://journals.ametsoc.org/doi/abs/10.1175/1520-0426(1986)003<0299:COAALA>2.0.CO;2) (Accessed 25 November 2013), 1986.
- 832 Giez, A.: Effective test and calibration of a trailing cone system on the atmospheric research aircraft HALO,
833 *Proceedings of the 56th Annual Symposium of the Society of Experimental Test Pilots*, Sep. 2012, 2012.
- 834 Goldenstein, C. S., Strand, C. L., Schultz, I. a, Sun, K., Jeffries, J. B. and Hanson, R. K.: Fitting of calibration-
835 free scanned-wavelength-modulation spectroscopy spectra for determination of gas properties and
836 absorption lineshapes., *Applied optics*, 53(3), 356–67, doi:10.1364/AO.53.000356, 2014.



- 837 Gurlit, W., Zimmermann, R., Giesemann, C., Fernholz, T., Ebert, V., Wolfrum, J., Platt, U. U. and Burrows, J.
838 P.: Lightweight diode laser spectrometer “CHILD” for balloon- borne measurements of water vapor and
839 methane, *Applied optics*, 44(1), 91–102, doi:10.1364/AO.44.000091, 2005.
- 840 Hansford, G. M., Freshwater, R. A., Eden, L., Turnbull, K. F. V., Hadaway, D. E., Ostanin, V. P. and Jones, R.
841 L.: Lightweight dew-/frost-point hygrometer based on a surface-acoustic-wave sensor for balloon-borne
842 atmospheric water vapor profile sounding, *Review of scientific instruments*, 77, 014502–014502,
843 doi:10.1063/1.2140275, 2006.
- 844 Held, I. and Soden, B.: Water vapor feedback and global warming, *Annual review of energy and the*
845 *environment*, 25(1), 441–475, doi:10.1146/annurev.energy.25.1.441, 2000.
- 846 Helten, M., Smit, H. G. J., Sträter, W., Kley, D., Nedelec, P., Zöger, M. and Busen, R.: Calibration and
847 performance of automatic compact instrumentation for the measurement of relative humidity from
848 passenger aircraft, *Journal of Geophysical Research: Atmospheres*, 103(D19), 25643–25652,
849 doi:10.1029/98JD00536, 1998.
- 850 Hoff, A.: WVSS-II Assessment at the DWD Deutscher Wetterdienst / German Meteorological Service
851 Climate Chamber of the Meteorological Observatory Lindenberg, Deutscher Wetterdienst, 2009.
- 852 Houghton, J.: *Global warming: The complete briefing*, Cambridge University Press. [online] Available from:
853 <http://britastro.org/jbaa/pdf/114-6shanklin.pdf> (Accessed 14 May 2014), 2009.
- 854 Hovde, D., Hodges, J., Scace, G. and Silver, J.: Wavelength-modulation laser hygrometer for ultrasensitive
855 detection of water vapor in semiconductor gases, *Applied optics*, 40(6), 829–839, doi:10.1364/AO.40.000829,
856 2001.
- 857 Hunsmann, S., Wagner, S., Saathoff, H., Möhler, O., Schurath, U. and Ebert, V.: Messung der
858 Temperaturabhängigkeit der Linienstärken und Druckverbreiterungskoeffizienten von H₂O-
859 Absorptionslinien im 1.4µm Band, in *VDI Berichte (1959)* VDI Verlag, Düsseldorf, pp. 149–164., 2006.
- 860 Hunsmann, S., Wunderle, K., Wagner, S., Rascher, U., Schurr, U. and Ebert, V.: Absolute, high resolution
861 water transpiration rate measurements on single plant leaves via tunable diode laser absorption
862 spectroscopy (TDLAS) at 1.37 µm, *Applied Physics B*, 92(3), 393–401, doi:10.1007/s00340-008-3095-2, 2008.
- 863 JCGM 2008: JCGM 200 : 2008 International vocabulary of metrology – Basic and general concepts and
864 associated terms (VIM) Vocabulaire international de métrologie – Concepts fondamentaux et généraux et
865 termes associés (VIM), International Organization for Standardization, 3(Vim), 104, doi:10.1016/0263-
866 2241(85)90006-5, 2008.
- 867 Joint Committee for Guides in Metrology (JCGM): Evaluation of measurement data - Guide to the
868 expression of uncertainty in measurement JCGM 100:2008, BIPM: Bureau International des Poids et
869 Mesures, www.bipm.org, 2008.
- 870 Joint Committee for Guides in Metrology (JCGM): Evaluation of measurement data - An introduction to the
871 “Guide to the expression of uncertainty in measurement” and related documents, BIPM: Bureau
872 International des Poids et Mesures, www.bipm.org, 2009.
- 873 Karpechko, A. Y., Perlwitz, J. and Manzini, E.: *Journal of Geophysical Research : Atmospheres*, , 1–16,
874 doi:10.1002/2013JD021350.Received, 2014.
- 875 Kaufmann, S., Voigt, C., Jurkat, T., Thornberry, T., Fahey, D. W., Gao, R.-S., Schlage, R., Schäuble, D. and
876 Zöger, M.: The airborne mass spectrometer AIMS – Part 1: AIMS-H₂O for UTLS water vapor
877 measurements, *Atmospheric Measurement Techniques*, 9(3), 939–953, doi:10.5194/amt-9-939-2016, 2016.
- 878 Kiehl, J. T. and Trenberth, K. E.: Earth’s Annual Global Mean Energy Budget, *Bulletin of the American*
879 *Meteorological Society*, 78(2), 197–208, doi:10.1175/1520-0477(1997)078<0197:EAGMEB>2.0.CO;2, 1997.
- 880 Kiemle, C., Schäfler, A. and Voigt, C.: Detection and analysis of water vapor transport, in *Atmospheric*
881 *Physics*, pp. 169–184, Springer Berlin Heidelberg., 2012.
- 882 Kley, D. and Stone, E.: Measurement of water vapor in the stratosphere by photodissociation with Ly α
883 (1216 Å) light, *Review of Scientific Instruments*, 49(6), 691, doi:10.1063/1.1135596, 1978.
- 884 Klostermann, T.: *Entwicklung und Erprobung des Hygrometer for Atmospheric Investigations*, Schriften
Page 23



- 885 des Forschungszentrums Jülich : Energie & Umwelt / Energy & Environment, 113, 2011.
- 886 Krämer, M., Schiller, C., Afchine, A., Bauer, R., Gensch, I., Mangold, A., Schlicht, S., Spelten, N., Sitnikov,
887 N., Borrmann, S., Reus, M. de and Spichtinger, P.: Ice supersaturations and cirrus cloud crystal numbers,
888 Atmospheric and Oceanic Optics, 9, 3505–3522, doi:10.5194/acp-9-3505-2009, 2009.
- 889 Krautstrunk, M. and Giez, A.: The Transition From FALCON to HALO Era Airborne Atmospheric
890 Research, in Atmospheric Physics, edited by U. Schumann, pp. 609–624., 2012.
- 891 Kühnreich, B., Klein, A., Höh, M., Buchholz, B. and Ebert, V.: Kompakte, direkt fasergekoppelte Multipass-
892 Zellen für spektroskopische Anwendungen im NIR-und MIR-Bereich, in DGAO Proceedings. [online]
893 Available from: http://www.dgao-proceedings.de/download/114/114_p35.pdf (Accessed 11 October 2013),
894 2013.
- 895 Lackner, M.: Tunable diode laser absorption spectroscopy (TDLAS) in the process industries – a review,
896 Reviews in Chemical Engineering, 23(2), 65–147, doi:10.1515/REVCE.2007.23.2.65, 2011.
- 897 Lockwood, J. G.: Clouds and the atmospheric radiation balance, Progress in Physical Geography, 14(1), 89–
898 96, doi:10.1177/030913339001400106, 1990.
- 899 Lu, E. and Takle, E. S.: Spatial variabilities and their relationships of the trends of temperature, water vapor,
900 and precipitation in the North American Regional Reanalysis, Journal of Geophysical Research, 115(D6),
901 D06110, doi:10.1029/2009JD013192, 2010.
- 902 Lübken, F.-J., Dingler, F., Lucke, H. von, Anders, J., Riedel, W. J. and Wolf, H.: MASERATI: a rocketborne
903 tunable diode laser absorption spectrometer, Applied optics, 38(25), 5338–5349, doi:10.1364/AO.38.005338,
904 1999.
- 905 Ludlam, F.: Clouds and storms: The behavior and effect of water in the atmosphere. [online] Available
906 from: <http://agris.fao.org/agris-search/search.do?recordID=US8025686> (Accessed 24 May 2014), 1980.
- 907 Mackrodt, P.: A New Attempt on a Coulometric Trace Humidity Generator, International Journal of
908 Thermophysics, 33(8-9), 1520–1535, doi:10.1007/s10765-012-1348-0, 2012.
- 909 Mangold, A. and Wodca Team: Intercomparison of water vapour detectors under field and defined
910 conditions, EGS-AGU-EUG Joint Assembly, (abstract 9330) [online] Available from:
911 <http://adsabs.harvard.edu/abs/2003EAEJA.....9330M> (Accessed 1 March 2014), 2003.
- 912 Marengo, A., Thouret, V., Nédélec, P., Smit, H., Helten, M., Kley, D., Karcher, F., Simon, P., Law, K., Pyle, J.,
913 Poschmann, G., Wrede, R. Von, Hume, C. and Cook, T.: Measurement of ozone and water vapor by Airbus
914 in-service aircraft: The MOZAIK airborne program, An overview, Journal of Geophysical Research,
915 103(D19), 25631–25642, doi:10.1029/98JD00977, 1998.
- 916 May, R. D.: Open-path, near-infrared tunable diode laser spectrometer for atmospheric measurements of
917 H₂O, Journal of Geophysical Research, 103(D15), 19161–19172, doi:10.1029/98JD01678, 1998.
- 918 Maycock, A. C., Shine, K. P. and Joshi, M. M.: The temperature response to stratospheric water vapour
919 changes, Quarterly Journal of the Royal Meteorological Society, 137, 1070–1082, doi:10.1002/qj.822, 2011.
- 920 McCarthy, M. P., Thorne, P. W. and Titchner, H. a.: An Analysis of Tropospheric Humidity Trends from
921 Radiosondes, Journal of Climate, 22(22), 5820–5838, doi:10.1175/2009JCLI2879.1, 2009.
- 922 McManus, J., Kebabian, P. and Zahniser, M.: Astigmatic mirror multipass absorption cells for long-path-
923 length spectroscopy, Applied Optics, 34(18), 3336–3348, doi:10.1364/AO.34.003336, 1995.
- 924 Meyer, J., Rolf, C., Schiller, C., Rohs, S., Spelten, N., Afchine, A., Zöger, M., Sitnikov, N., Thornberry, T. D.,
925 Rollins, A. W., Bozoki, Z., Tatrai, D., Ebert, V., Kühnreich, B., Mackrodt, P., Möhler, O., Saathoff, H.,
926 Rosenlof, K. H. and Krämer, M.: Two decades of water vapor measurements with the FISH fluorescence
927 hygrometer: A review, Atmospheric Chemistry and Physics, 15(14), 8521–8538, doi:10.5194/acp-15-8521-
928 2015, 2015.
- 929 Mihalcea, R., Baer, D. and Hanson, R.: Diode laser sensor for measurements of CO, CO₂, and CH₄ in
930 combustion flows, Applied Optics, 36(33), 8745–8752, doi:10.1364/AO.36.008745, 1997.
- 931 Miloshevich, L. M., Vömel, H., Whiteman, D. N., Lesht, B. M., Schmidlin, F. J. and Russo, F.: Absolute



- 932 accuracy of water vapor measurements from six operational radiosonde types launched during AWEX-G
933 and implications for AIRS validation, *Journal of Geophysical Research: Atmospheres*, 111(D9),
934 doi:10.1029/2005JD006083, 2006.
- 935 Möller, D., Feichter, J. and Herrmann, H.: Von Wolken, Nebel und Niederschlag, in *Chemie über den*
936 *Wolken:... und darunter*, edited by R. Zellner, pp. 236–240, WILEY-VCH Verlag GmbH & Co. KGaA,
937 Weinheim., 2011.
- 938 Muecke, R. J., Scheumann, B., Slemr, F. and Werle, P. W.: Calibration procedures for tunable diode laser
939 spectrometers, *Proc. SPIE 2112, Tunable Diode Laser Spectroscopy, Lidar, and DIAL Techniques for*
940 *Environmental and Industrial Measurement*, 2112, 87–98, doi:10.1117/12.177289, 1994.
- 941 Oelhaf, H., Fix, A., Schiller, C. and Chance, K.: Validation of MIPAS-ENVISAT Version 4.61 Operational
942 Data with Balloon and Aircraft Measurements: H₂O, *Chemistry Validation, 2004(August)*, 3–7 [online]
943 Available from: <http://earth.esa.int/envisat/workshops/acve2/papers/EMI02HO1.pdf> (Accessed 22 January
944 2012), 2004.
- 945 Ohtaki, E. and Matsui, T.: Infrared device for simultaneous measurement of fluctuations of atmospheric
946 carbon dioxide and water vapor, *Boundary-Layer Meteorology*, 24(1), 109–119, doi:10.1007/BF00121803,
947 1982.
- 948 Oltmans, S. and Hofmann, D.: Increase in lower-stratospheric water vapour at a mid-latitude Northern
949 Hemisphere site from 1981 to 1994, *Nature*, 374, 146–149, doi:10.1038/374146a0, 1995.
- 950 Peter, T., Marcolli, C., Spichtinger, P., Corti, T., Baker, M. B. and Koop, T.: When dry air is too humid,
951 *Science*, 314(5804), 1399–1402, doi:10.1126/science.1135199, 2006.
- 952 Petersen, R., Crouce, L., Feltz, W., Olson, E. and Helms, D.: WVSS-II moisture observations: A tool for
953 validating and monitoring satellite moisture data, *EUMETSAT Meteorological Satellite Conference*, 22, 67–
954 77 [online] Available from:
955 http://www.eumetsat.int/Home/Main/AboutEUMETSAT/Publications/ConferenceandWorkshopProceedings/2010/groups/cps/documents/document/pdf_conf_p57_s1_03_petersen_v.pdf (Accessed 20 January 2012),
956 2010.
957
- 958 Podolske, J. and Loewenstein, M.: Airborne tunable diode laser spectrometer for trace-gas measurement in
959 the lower stratosphere, *Applied optics*, 32(27), 5324–5333, doi:10.1364/AO.32.005324., 1993.
- 960 Podolske, J., Sachse, G. and Diskin, G.: Calibration and data retrieval algorithms for the NASA
961 Langley/Ames Diode Laser Hygrometer for the NASA Transport and Chemical Evolution Over the Pacific
962 (TRACE-P) mission, *Journal of Geophysical Research*, 108(D20), 8792, doi:10.1029/2002JD003156, 2003.
- 963 Ramanathan, V., Cess, R. D., Harrison, E. F., Minnis, P., Barkstrom, B. R., Ahmad, E. and Hartmann, D.:
964 Cloud-radiative forcing and climate: results from the Earth radiation budget experiment, *Science (New*
965 *York, N.Y.)*, 243(4887), 57–63, doi:10.1126/science.243.4887.57, 1989.
- 966 Ravishankara, A. R.: Water Vapor in the Lower Stratosphere, *Science*, 337(6096), 809–810,
967 doi:10.1126/science.1227004, 2012.
- 968 Rieker, G., Jeffries, J. and Hanson, R.: Calibration-free wavelength-modulation spectroscopy for
969 measurements of gas temperature and concentration in harsh environments, *Applied optics*, 48(29), 5546–
970 5560, doi:10.1364/AO.48.005546, 2009.
- 971 Rollins, A., Thornberry, T., Gao, R. S., Smith, J. B., Sayres, D. S., Sargent, M. R., Schiller, C., Krämer, M.,
972 Spelten, N., Hurst, D. F., Jordan, A. F., Hall, E. G., Vömel, H., Diskin, G. S., Podolske, J. R., Christensen, L.
973 E., Rosenlof, K. H., Jensen, E. J. and Fahey, D. W.: Evaluation of UT/LS hygrometer accuracy by
974 intercomparison during the NASA MACPEX mission, *Journal of Geophysical Research: Atmospheres*, 119,
975 doi:10.1002/2013JD020817, 2014.
- 976 Rosenlof, K. H., Oltmans, S. J., Kley, D., III, J. M. R., Chiou, E.-W., Chu, W. P., Johnson, D. G., Kelly, K. K.,
977 Michelsen, H. A., Nedoluha, G. E., Remsberg, E. E., Toon, G. C. and McCormick, M. P.: Stratospheric water
978 vapor increases over the past half-century, *Geophysical Research Letters*, 28(7), 1195–1198,
979 doi:10.1029/2000GL012502, 2001.



- 980 Ross, R. and Elliott, W.: Tropospheric water vapor climatology and trends over North America: 1973-93,
981 *Journal of Climate*, 9(12), 3561–3574, doi:10.1175/1520-0442(1996)009<3561:TWVCAT>2.0.CO;2, 1996.
- 982 Rothman, L. S., Gordon, I. E., Barbe, A., Benner, D. C., Bernath, P. F., Birk, M., Boudon, V., Brown, L. R.,
983 Campargue, A. and Champion, J.-P.: The HITRAN 2008 molecular spectroscopic database, *Journal of*
984 *Quantitative Spectroscopy and Radiative Transfer*, 110(9-10), 533–572, doi:10.1016/j.jqsrt.2009.02.013, 2009.
- 985 Roths, J. and Busen, R.: Development of a laser in situ airborne hygrometer (LISAH) (feasibility study),
986 *Infrared physics & technology*, 37(1), 33–38, doi:10.1016/1350-4495(95)00103-4, 1996.
- 987 Salasmaa, E. and Kostamo, P.: HUMICAP® thin film humidity sensor, in *Advanced Agricultural*
988 *Instrumentation Series E: Applied Sciences*, edited by W. G. Gensler, pp. 135–147, Kluwer., 1986.
- 989 Sargent, M. R., Sayres, D. S., Smith, J. B., Witinski, M., Allen, N. T., Demusz, J. N., Rivero, M., Tuozzolo, C.
990 and Anderson, J. G.: A new direct absorption tunable diode laser spectrometer for high precision
991 measurement of water vapor in the upper troposphere and lower stratosphere, *Review of Scientific*
992 *Instruments*, 84(7), 074102, doi:10.1063/1.4815828, 2013.
- 993 Schäfler, A., Dörrnbrack, A., Kiemle, C., Rahm, S., Wirth, M., Schäfler, A. and Dörrnbrack, A.: Tropospheric
994 Water Vapor Transport as Determined from Airborne Lidar Measurements, *Journal of Atmospheric &*
995 *Oceanic Technology*, 27(12), 2017–2030, doi:10.1175/2010JTECHA1418.1, 2010.
- 996 Scherer, M., Vömel, H., Fueglistaler, S., Oltmans, S. J. and Staehelin, J.: Trends and variability of midlatitude
997 stratospheric water vapour deduced from the re-evaluated Boulder balloon series and HALOE,
998 *Atmospheric Chemistry and Physics*, 8, 1391–1402, doi:10.5194/acp-8-1391-2008, 2008.
- 999 Schiff, H. I., Mackay, G. I. and Bechara, J.: The use of tunable diode laser absorption spectroscopy for
1000 atmospheric measurements, *Research on chemical intermediates*, 20(3), 525–556,
1001 doi:10.1163/156856794X00441, 1994.
- 1002 Schlager, H.: ESMVal (Earth System Model Validation), <http://www.pa.op.dlr.de/ESMVal> (last accessed:
1003 May 2014), 2014.
- 1004 Schlosser, H. E., Fernholz, T., Teichert, H. and Ebert, V.: In situ detection of potassium atoms in high-
1005 temperature coal-combustion systems using near-infrared-diode lasers, *Spectrochimica Acta Part A:*
1006 *Molecular and Biomolecular Spectroscopy*, 58(11), 2347–2359, doi:10.1016/S1386-1425(02)00049-5, 2002.
- 1007 Schneider, S.: Cloudiness as a global climatic feedback mechanism: The effects on the radiation balance and
1008 surface temperature of variations in cloudiness, *Journal of the Atmospheric Sciences*, 29(8), 1413–1422,
1009 doi:10.1175/1520-0469(1972)029<1413:CAAGCF>2.0.CO;2, 1972.
- 1010 Schulz, C., Dreizler, A., Ebert, V. and Wolfrum, J.: Combustion Diagnostics, in *Handbook of Experimental*
1011 *Fluid Mechanics*, edited by C. Tropea, A. L. Yarin, and J. F. Foss, pp. 1241–1316, Springer Berlin Heidelberg,
1012 Heidelberg., 2007.
- 1013 Seidel, A., Wagner, S. and Ebert, V.: TDLAS-based open-path laser hygrometer using simple reflective foils
1014 as scattering targets, *Applied Physics B*, 109(3), 497–504, doi:10.1007/s00340-012-5228-x, 2012.
- 1015 Sherwood, S., Bony, S. and Dufresne, J.: Spread in model climate sensitivity traced to atmospheric
1016 convective mixing, *Nature*, 505(7481), 37–42, doi:10.1038/nature12829, 2014.
- 1017 Silver, J. and Hovde, D.: Near-infrared diode laser airborne hygrometer, *Review of scientific instruments*,
1018 65, 5, 1691–1694 [online] Available from: http://ieeexplore.ieee.org/xpls/abs_all.jsp?arnumber=4991817
1019 (Accessed 25 November 2013a), 1994.
- 1020 Silver, J. and Zondlo, M.: High-precision CO₂ sensor for meteorological balloons, in *SPIE Proceedings 6378,*
1021 *Chemical and Biological Sensors for Industrial and Environmental Monitoring II*, 6378J., 2006.
- 1022 Silver, J. A.: Frequency-modulation spectroscopy for trace species detection: theory and comparison among
1023 experimental methods: errata, *Applied optics*, 31(24), 4927–4927, doi:10.1364/AO.31.004927, 1992.
- 1024 Silver, J. A. and Hovde, D. C.: Near-infrared diode laser airborne hygrometer, *Review of scientific*
1025 *instruments*, 65(5), 1691–1694, doi:10.1063/1.1144861, 1994b.
- 1026 Smit, H. G. J., Strater, W., Helten, M. and Kley, D.: Environmental simulation facility to calibrate airborne



- 1027 ozone and humidity sensors, in Forschungszentrum Jülich Berichte 3796, Forschungszentrum Jülich,
1028 Zentralbibliothek. [online] Available from: <http://www.opengrey.eu/item/display/10068/253740> (Accessed
1029 25 November 2013), 2000.
- 1030 Smit, H. G. J., Rolf, C., Kraemer, M., Petzold, A., Spelten, N., Neis, P., Maser, R., Buchholz, B., Ebert, V. and
1031 Tatrai, D.: Development and Evaluation of Novel and Compact Hygrometer for Airborne Research
1032 (DENCHAR): In-Flight Performance During AIRTOSS-I / II Research Aircraft Campaigns, Geophysical
1033 Research Abstracts, 16(EGU2014-9420), 2014.
- 1034 Smorgon, D., Boese, N., Ebert, V. and Team, A.: Airborne hygrometer calibration inter-comparison against a
1035 metrological water vapour standard, Geophysical Research Abstracts, 16(EGU2014-5929), 2014.
- 1036 Solomon, S., Rosenlof, K. H., Portmann, R. W., Daniel, J. S., Davis, S. M., Sanford, T. J. and Plattner, G.-K.:
1037 Contributions of stratospheric water vapor to decadal changes in the rate of global warming, *Science* (New
1038 York, N.Y.), 327(5970), 1219–23, doi:10.1126/science.1182488, 2010.
- 1039 Spichtinger, P., Gierens, K., Smit, H. G. J., Ovarlez, J. and Gayet, J.-F.: On the distribution of relative
1040 humidity in cirrus clouds, *Atmospheric Chemistry and Physics*, 4, 639–647, doi:10.5194/acp-4-639-2004,
1041 2004.
- 1042 Sun, K., Sur, R., Chao, X., Jeffries, J. B., Hanson, R. K., Pummill, R. J. and Whitty, K. J.: TDL absorption
1043 sensors for gas temperature and concentrations in a high-pressure entrained-flow coal gasifier, *Proceedings
1044 of the Combustion Institute*, 34(2), 3593–3601, doi:10.1016/j.proci.2012.05.018, 2013.
- 1045 Szakáll, M., Bozóki, Z., Mohácsi, Á., Varga, T., Szabó, G. and Varga, A.: Diode laser based photoacoustic
1046 water vapor detection system for atmospheric research, *Applied Spectroscopy*, 58(7), 792–798,
1047 doi:10.1366/0003702041389373, 2004.
- 1048 Teichert, H., Fernholz, T. and Ebert, V.: Simultaneous in-situ measurement of CO, H₂O, and gas
1049 temperatures in a full-sized coal-fired power plant by near-infrared diode lasers, *Applied optics*, 42(12),
1050 2043–2051, doi:10.1364/AO.42.002043, 2003.
- 1051 Thornberry, T. D., Rollins, A. W., Gao, R. S., Watts, L. A., Ciciora, S. J., McLaughlin, R. J. and Fahey, D. W.:
1052 A two-channel, tunable diode laser-based hygrometer for measurement of water vapor and cirrus cloud ice
1053 water content in the upper troposphere and lower stratosphere, *Atmospheric Measurement Techniques
1054 Discussions*, 7(8), 8271–8309, doi:10.5194/amt-d-7-8271-2014, 2014.
- 1055 Trenberth, K. E., Fasullo, J. and Smith, L.: Trends and variability in column-integrated atmospheric water
1056 vapor, *Climate Dynamics*, 24(7-8), 741–758, doi:10.1007/s00382-005-0017-4, 2005.
- 1057 Vance, A. K., Woolley, A., Cotton, R., Turnbull, K., Abel, S. and Harlow, C.: Final Report on the WVSS-II
1058 Sensors fitted to the FAAM BAe 146, in Met Office, pp. 0–31, Met Office., 2011.
- 1059 Vance, A. K., Abel, S. J., Cotton, R. J. and Woolley, A. M.: Performance of WVSS-II hygrometers on the
1060 FAAM research aircraft, *Atmospheric Measurement Techniques*, 8(3), 1617–1625, doi:10.5194/amt-8-1617-
1061 2015, 2015.
- 1062 Vömel, H., David, D. and Smith, K.: Accuracy of tropospheric and stratospheric water vapor measurements
1063 by the cryogenic frost point hygrometer: Instrumental details and observations, *Journal of Geophysical
1064 Research: Atmospheres*, 112(D8), 1–14, doi:10.1029/2006JD007224, 2007.
- 1065 Wagner, S., Klein, M., Kathrotia, T. and Riedel, U.: Absolute, spatially resolved, in situ CO profiles in
1066 atmospheric laminar counter-flow diffusion flames using 2.3 μm TDLAS, *Applied Physics B*, 109(3), 533–
1067 540, doi:10.1007/s00340-012-5242-z, 2012.
- 1068 Webster, C., Flesch, G., Mansour, K., Haberle, R. and Bauman, J.: Mars laser hygrometer, *Applied optics*,
1069 43(22), 4436–4445, doi:10.1364/AO.43.004436, 2004.
- 1070 Weinstock, E., Hints, E. J., Dessler, A. E., Oliver, J. F., Hazen, N. L., Demusz, J. N., Allen, N. T., Lapson, L.
1071 B. and Anderson, J. G.: New fast response photofragment fluorescence hygrometer for use on the NASA
1072 ER-2 and the Perseus remotely piloted aircraft, *Review of scientific instruments*, 65(11), 3544 – 3554,
1073 doi:10.1063/1.1144536, 1994.
- 1074 Werle, P.: A review of recent advances in semiconductor laser based gas monitors, *Spectrochimica Acta Part*



- 1075 A: Molecular and Biomolecular Spectroscopy, 54(2), 197–236, doi:10.1016/S1386-1425(97)00227-8, 1998.
- 1076 White, J.: Very long optical paths in air, Journal of the Optical Society of America (1917-1983), 66(5), 411–
1077 416, doi:10.1364/JOSA.66.000411, 1976.
- 1078 Wiederhold, P. R.: Water Vapor Measurement. Methods and Instrumentation, Har/Dskt., CRC Press., 1997.
- 1079 Witzel, O., Klein, A., Wagner, S., Meffert, C., Schulz, C. and Ebert, V.: High-speed tunable diode laser
1080 absorption spectroscopy for sampling-free in-cylinder water vapor concentration measurements in an
1081 optical IC engine, Applied Physics B, 109(3), 521–532, doi:10.1007/s00340-012-5225-0, 2012.
- 1082 Witzel, O., Klein, A., Meffert, C., Wagner, S., Meffert, C., Schulz, C. and Ebert, V.: VCSEL-based, high-
1083 speed, in situ TDLAS for in-cylinder water vapor measurements in IC engines, Optics express, 21(17),
1084 19951–19965, doi:10.1364/OE.21.019951, 2013.
- 1085 Wolfrum, J., Dreier, T., Ebert, V. and Schulz, C.: Laser-Based Combustion Diagnostics, in Encyclopedia of
1086 Analytical Chemistry, eds R.A. Meyers, John Wiley: Chichester. 2nd edition, p. 33., 2011.
- 1087 Wunderle, K., Fernholz, T. and Ebert, V.: Selection of optimal absorption lines for tunable laser absorption
1088 spectrometers, VDI Berichte, 1959, 137–148, 2006.
- 1089 Wunderle, K., Al-Zaitone, B., Pašti, I., Wagner, S., Hunsmann, S., Tropea, C. and Ebert, V.: TDLAS-
1090 Spektrometer zur räumlich aufgelösten absoluten Wasserdampfbestimmung um akustisch levitierte
1091 Einzeltröpfchen, in VDI Berichte (2047) VDI Verlag, Düsseldorf, pp. 103–112., 2008.
- 1092 Xie, B., Zhang, Q. and Ying, Y.: Trends in Precipitable Water and Relative Humidity in China: 1979–2005,
1093 Journal of Applied Meteorology and Climatology, 50(10), 1985–1994, doi:10.1175/2011JAMC2446.1, 2011.
- 1094 Zachariassen, J., Zeller, K., Nikolov, N. and McClelland, T.: A review of the forest service remote automated
1095 weather station (RAWS) network, in General Technical Report RMRS-GTR-119. Fort Collins, CO: USDA
1096 Forest Service, Rocky Mountain Research Station, US Department of Agriculture, Forest Service, Rocky
1097 Mountain Research Station. [online] Available from: http://www.fs.fed.us/rm/pubs/rmrs_gtr119.pdf
1098 (Accessed 13 February 2012), 2003.
- 1099 Zöger, M., Engel, A., McKenna, D. S., Schiller, C., Schmidt, U. and Woyke, T.: Balloon-borne in situ
1100 measurements of stratospheric H₂O, CH₄ and H₂ at midlatitudes, Journal of Geophysical Research,
1101 104(D1), 1817–1825, doi:10.1029/1998JD100024, 1999a.
- 1102 Zöger, M., Afchine, A., Eicke, N., Gerhards, M.-T., Klein, E., McKenna, D. S., Mörschel, U., Schmidt, U., Tan,
1103 V., Tuitjer, F., Woyke, T. and Schiller, C.: Fast in situ stratospheric hygrometers: A new family of balloon-
1104 borne and airborne Lyman photofragment fluorescence hygrometers, Journal of Geophysical Research,
1105 104(D1), 1807–1816, doi:10.1029/1998JD100025, 1999b.
- 1106 Zondlo, M., Paige, M. E., Massick, S. M. and Silver, J.: Vertical cavity laser hygrometer for the National
1107 Science Foundation Gulfstream-V aircraft, Journal of Geophysical Research, 115(D20), 20309,
1108 doi:10.1029/2010JD014445, 2010.

1109

1110 **Figures:**

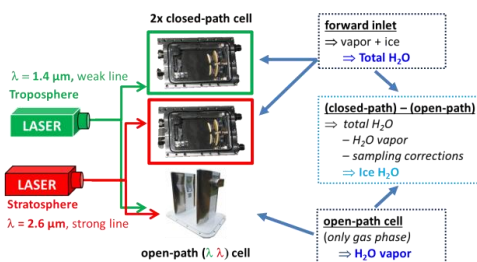
1111

1112



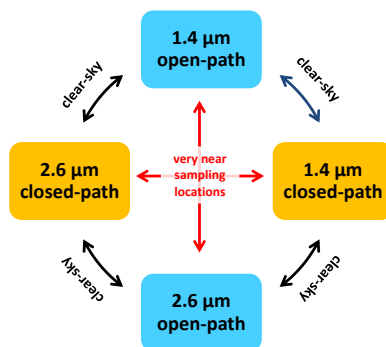
1129 Figure 3: Photos from the cabin layout of HALO with payload of the TACTS/ESMVal campaign (left). Photo of the fuse-
 1130 lage of HALO showing the trace gas inlet (TGI) for the closed-path HAI cells (for total water detection) as well as the
 1131 open-path HAI cell (for gas phase water detection; yellow marked are the open laser beams)

1132
 1133
 1134



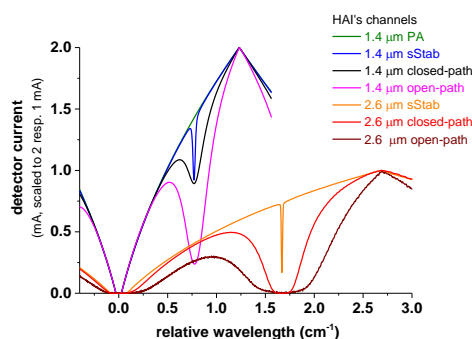
1135 Figure 4: Schematic of HAI's working principle in the multi-phase configuration. By combining selective open-path gas
 1136 phase measurements with total water measurements in the closed-path, extractive cell (ice is evaporated before the cell
 1137 by heated inlet lines), it is possible to derive the ice water content from the difference between closed-path and open-
 1138 path readings.
 1139

1140
 1141
 1142
 1143



1144 Figure 5: Self-validation possibilities of HAI under clear-sky conditions (black) and redundancies under all atmospheric
 1145 conditions (red). For details see text.
 1146

1147



1148
 1149 Figure 6: dTDLAS raw signals (spectra) of all seven spectroscopic channels permanently acquired and saved by HAI.
 1150 The x-axis is already converted to the wavelength axis via the dynamic tuning rate of the laser. Each spectrum contains
 1151 approx. 1700 16-bit values. (PA: parasitic absorption, sStab: spectral stabilization)

1152

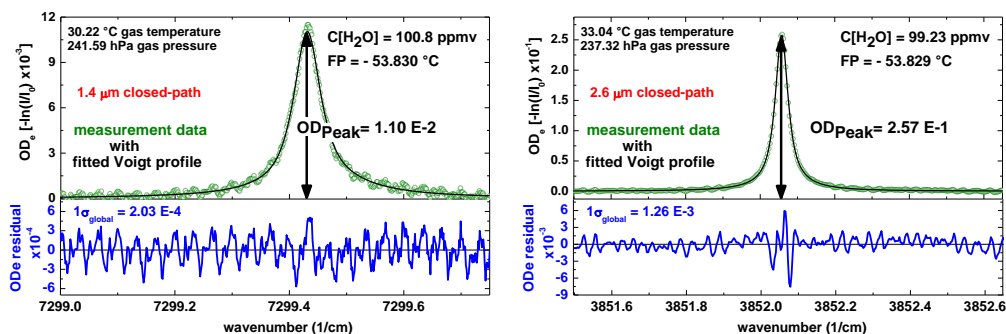


Figure 7: Typical pre-processed absorption signals (after baseline, offset and transmission correction) for both closed-path spectrometer channels (right 1.4 μm left: 2.6 μm) during flight. The laser modulation frequency was 240 Hz. 50 individual raw scans are pre-averaged yielding 4.8 H₂O measurements per second with 69 ms total integration time. This corresponds to a spatial resolution of 15 m at 800 km/h cursing speed. Without averaging, HAI achieves a maximum time resolution of 1.3 ms, respectively a spatial resolution of 30 cm at 800 km/h cursing speed. (It should be noted that the four vertical axes have different scales).

1153

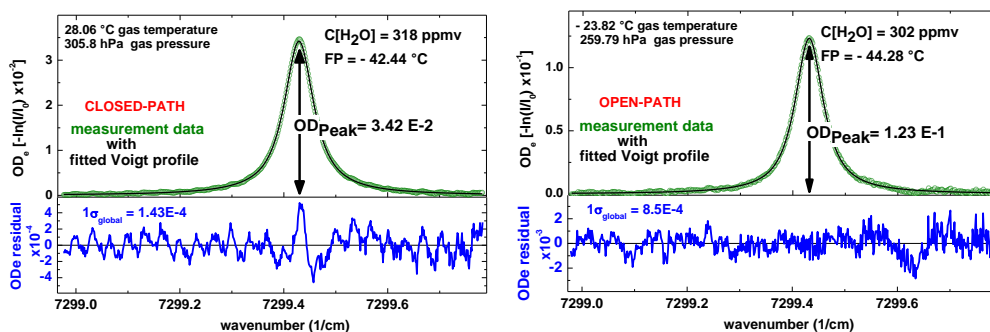


Figure 8: Comparison of pre-processed TDLAS scans (similar to Figure 7) of HAI's 1.4 μm closed-path (left) and the 1.4 μm open-path cell (right) during a HALO flight. Despite the entirely different measurement conditions such as wind speed (cm/s to 100 m/s) or temperature (+28 $^{\circ}\text{C}$ to -23 $^{\circ}\text{C}$), both channels are evaluated calibration-free with the exact same methods and model.

1154

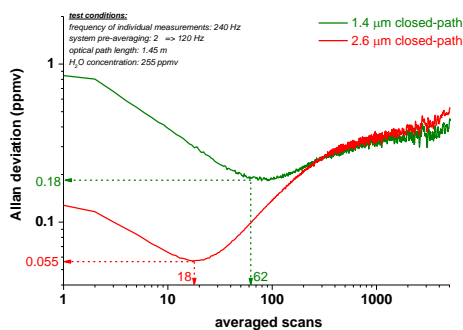
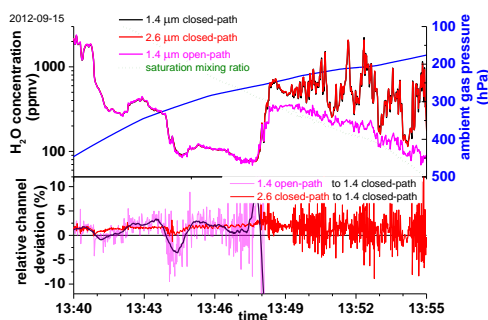


Figure 9: Allan variance plots for both closed-path spectrometer channels. The measurements were done by analysing gas from a big buffer vessel with a H_2O concentration of 255 ppmv. The optimal precision from this measurement is 0.22 ppmv for the 1.4 μm closed-path cell at 4.8 Hz (same as in Figure 7) and 0.065 ppmv for the 2.6 μm closed-path cell. The best i.e. highest precision of 0.18 ppmv is achieved at 3.8 Hz for the 1.4 μm cell and 0.055 ppmv at 13 Hz for the 2.6 μm cell.

1155

1156



1157
1158 Figure 10: Typical HAI measurement on board HALO during the TACTS/ESMVal campaign. The flight
1159 profile shows a 15 min section of a slow ascent from the lower troposphere to the upper troposphere. The
1160 first part (under clear sky condition) can be used to perform an absolute in-flight accuracy validation of
1161 both closed-path channels of HAI; the second part on the right side demonstrates a HAI multi-phase H₂O
1162 measurement. For further explanations of all signals and visible effects see text.
1163